Test of the LHC Diamond Beam Loss Monitors

E. Griesmayer, CIVIDEC Instrumentation (corresponding author)
B. Dehning, E. Effinger, CERN BE/BI
H. Pernegger, D. Dobos, CERN PH

Draft version, 1.3.2011

Abstract

Chemical Vapour Deposition (CVD) diamond detectors were installed in the collimation area of the CERN LHC to study their feasibility as Fast Beam Loss Monitors in a high-radiation environment.

Four detectors were configured with fast, radiation-hard pre-amplifiers with a bandwidth of 2 GHz. The readout was via an oscilloscope with a bandwidth of 1 GHz and a sampling rate of 5 GSPS. Despite the 250 m cable run from the detectors to the oscilloscope, single MIPs were resolved with a 2 ns rise time, a pulse width of 10 ns and a time resolution of less than 880 ps.

Two modes of operation were applied. For the analysis of unexpected beam aborts, the loss profile was recorded in a 1 ms buffer and, for nominal operation, the histogram of the time structure of the losses was recorded in synchronism with the LHC period of 89.2 us.

Measurements during the LHC start-up (February to December 2010) are presented. The Diamond Monitors gave an unprecedented insight into the time structure of the beam losses resolving the LHC RF frequency of 400 MHz as well as the nominal bunch separation of 25 ns. In future, these detectors will be used to study ghost bunches and particles in the 3 us abort gap.

1. Measurement setup

1.1 Installation of the Diamond Beam Loss Monitors

Four Diamond Beam Loss Monitors (DBLM) were mounted in the LHC tunnel in the collimation area in IP7, one on the lefthand side (TCLA.D6L7.B2) and three on the righthand side (TCHSS.6R7.B2), each next to primary collimators (Figure 1).

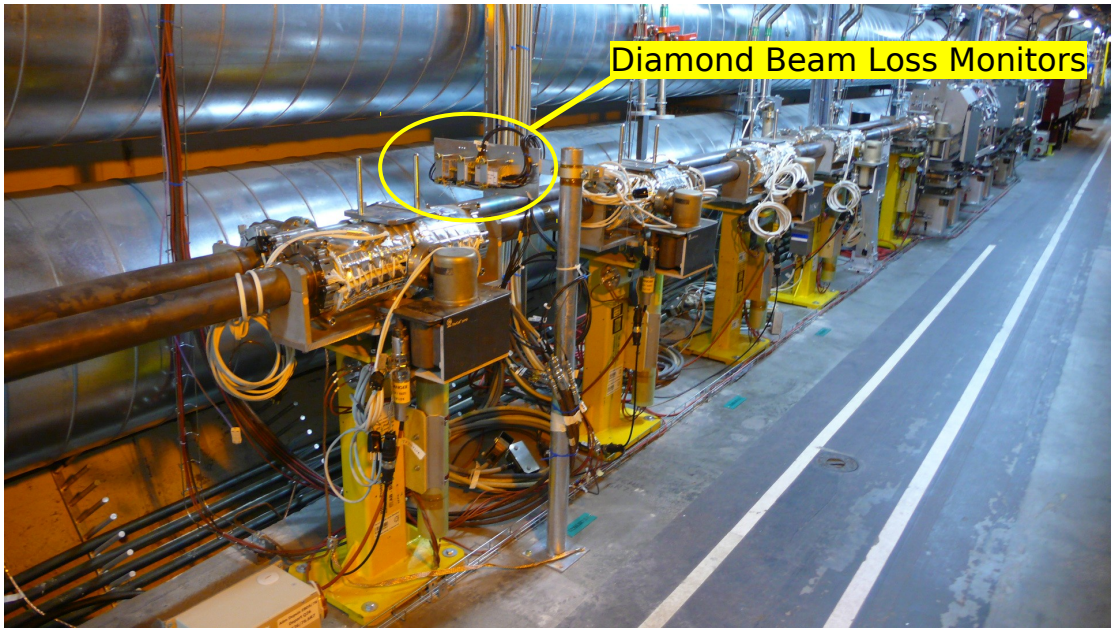

Figure 1: Location of the three detectors on the righthand side in the LHC IP7.

1.2 DBLM

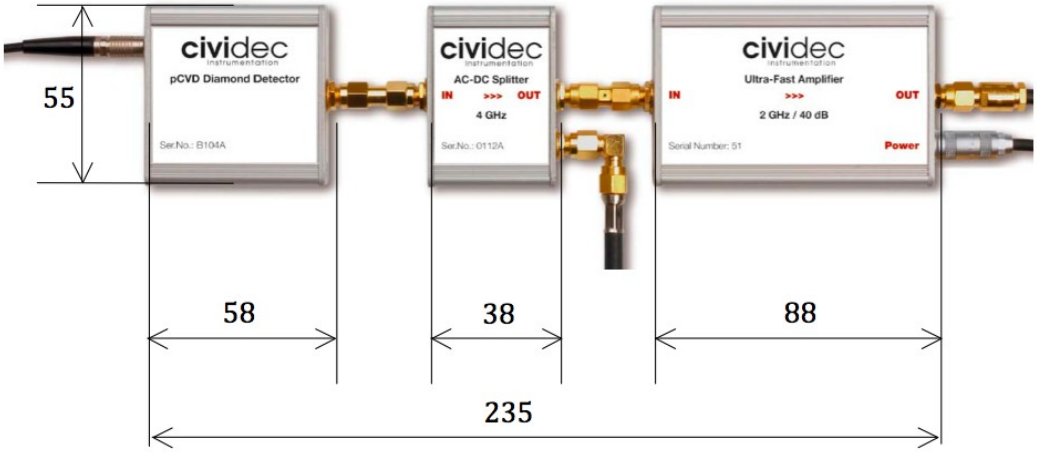

Figure 2: The DBLM consists of the diamond detector, an AC-DC splitter and a pre-amplifier.

The DBLM consists of the diamond detector, an AC-DC splitter and a pre-amplifier. The DBLM is mounted on an aluminium plate and a stand, which is screwed to the LHC tunnel floor. The stand is electrically connected to the LHC ground and the DBLM is electrically isolated from this ground point. The DBLM received its ground from the control room.

1.3 Diamond detector

The diamond detector consists of a 10 mm × 10 mm × 0.5 mm pCVD diamond substrate coated on each side with a 200 nm thick gold electrode with a size of 8 mm × 8 mm, Figure 3. The detector capacitance is typically 8 pF.

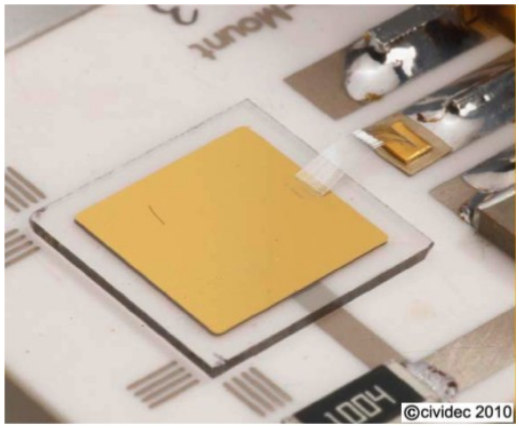

Figure 3: The diamond detector is mounted on a ceramic substrate and bonded to the readout line.

The bottom electrode is glued to a ceramic PCB and the top electrode is bonded with 10 um thick aluminium bonding wires. The detector is mounted in an aluminium box with extra RF shielding.

1.4 AC-DC splitter

The AC-DC Splitter decouples the detector's DC dark current from the AC signals. It has an analogue bandwidth of 4 GHz and provides the DC path to ground.

1.5 Pre-amplifier

A broadband current amplifier with a bandwidth of 2 GHz was used for the tests. This pre-amplifier is optimized for use with pCVD diamond detectors. It is radiation resistant up to 1 MGy and has a

dedicated input protection according to IEC61000-4-2 (±8 kV, 2 A for 1 µs). The pre-amplifier can intrinsically provide a rise time of 180 ps, a pulse width of 300 ps and a fall time of 400 ps, which is crucial for the measurement of the fast pulses from the diamond detector. Three channels were equipped with 40 dB pre-amplifiers and one channel with a 20 dB pre-amplifier.

1.6 Schematics

The schematic diagram in Figure 4 shows the overall monitor system set-up. The ionization charge from the detector appears as a current source on the high voltage side that is connected via a 1 MW load resistor and a 1.5 nF / 1 kV blocking capacitor.

The input of the pre-amplifier is ac-coupled with a 1.5 nF / 1 kV coupling capacitance to the 50 Ω input of the pre-amplifier. The output is AC coupled with 100 nF.

A 250 m long CK50 cable connects the detector to the instrumentation in the counting room where a bandpass filter with 200 kHz low cut-off frequency is used.

Data recording is done with a LeCroy oscilloscope with a bandwidth of 1 GHz and a sampling rate of 5 GSPS. For most measurements a 200 MHz bandwidth limitation was used.

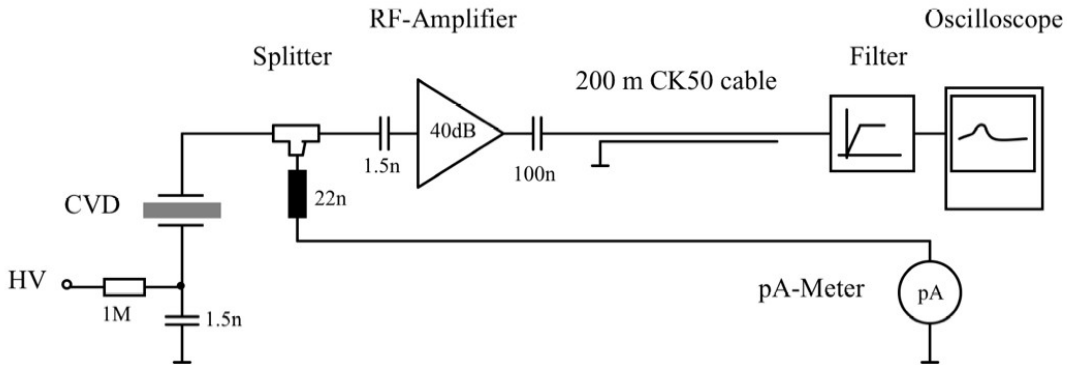

Figure 4: Schematic view of the overall DBLM.

2 Calibration

2.1 Principle

The ionization energy for CVD diamond is 13 eV/eh-pair and the stopping power for MIP particles is 615 eV/um[1]. The energy loss for MIP particles in the 500 um thick CVD detector is 308 keV and the deposited charge is 23'650 eh-pairs, which corresponds to 7.57 fC.

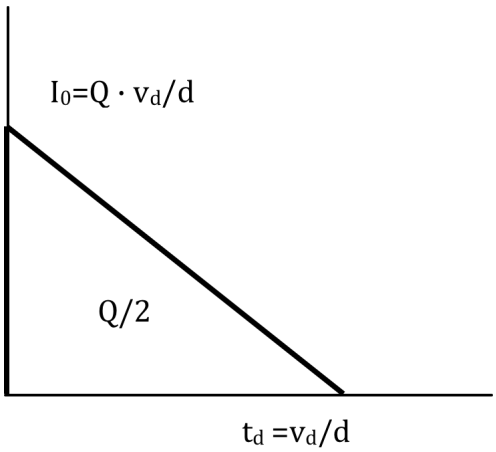

Figure 5: Ionization current for a MIP particle.

Integration of the ionization current of a MIP particle (Figure 5), shows that only half of this charge (3.78 fC) is seen by the electrode.

For pCVD diamond, the collected charge depends on the charge-collection distance (CCD), which is 200 um for the material used (note this less than the thickness of the detector). The effective charge read out by the pre-amplifier is 1.6 fC (equivalent to 10'000 charges).

2.2 Electronic calibration

The collected charge is used for the calibration of the detector in order to determine the signal-to-noise ratio (SNR), which defines the efficiency of single-MIP-particle detection.

The schematics for the electronic calibration is shown in Figure 6. A pulse generator provides the calibration voltage step u_{cal}, which is attenuated by -40 dB before being fed into the calibration capacitance C_{cal}, where it is converted into the calibration charge Q_{cal}, which is fed into the 40 dB pre-amplifier.

[1] Private communication: GEANT4 simulations by Pavel Kavrigin.

The generated pulse shape is equivalent to the pulse shape of a physics event, Figure 7.

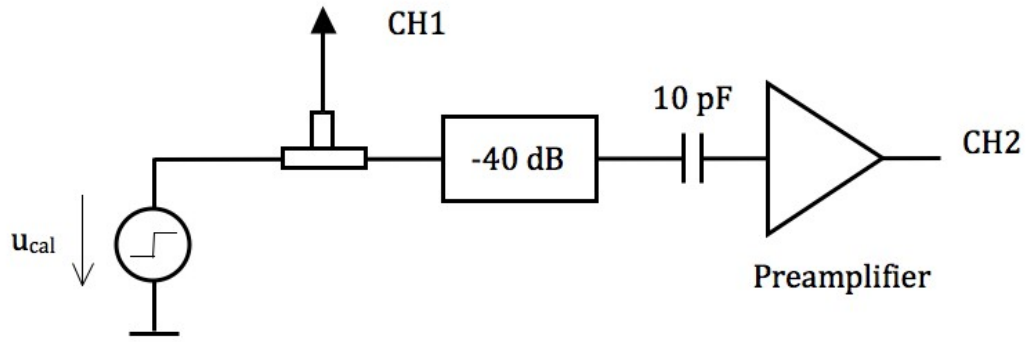

Figure 6: Schematic for SNR measurement.

The input voltage step is divided by a 50 Ω signal splitter, attenuated by -40 dB and fed into the capacitor and the +40 dB pre-amplifier.

The signal-to-noise ratio SNR is defined by the ratio of the amplitude v_2 and the rms baseline noise $v_{noise,\ rms}$:

SNR = v_2 / $v_{noise,\ rms}$

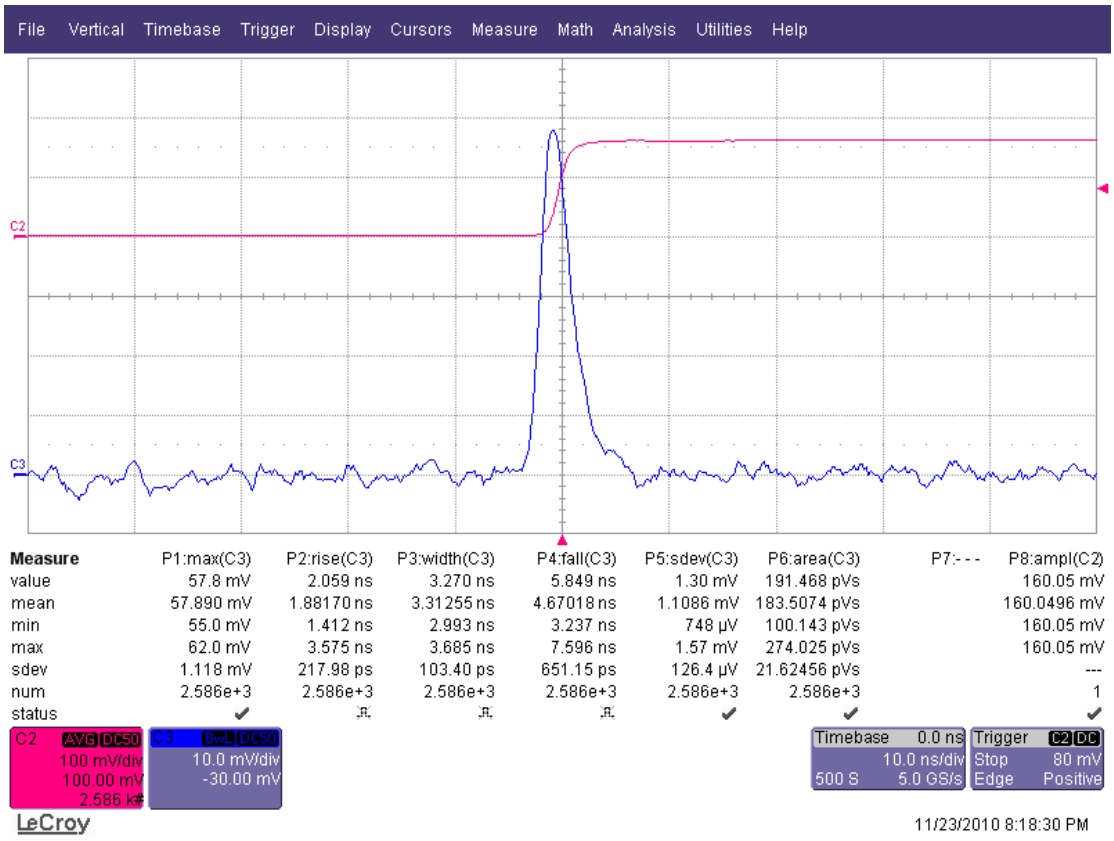

Figure 7: Calibration pulse as a response to a calibration voltage step.

The calibration charge $Q_{cal} = v_{cal} \times u_{cal}$ = 160 mV × 10 pF = 16 fC. This is equivalent to 100'000 electrons, and to 10 MIP.

The SNR for 1 MIP particle is:

SNR = v_2 / $v_{noise,\ rms}$ / 10 = 57.890 mV/1.1086 mV/10 = 5.22

The SNR of the detector is 5.22 for single MIP particles with 1.6 fC.

2.3 Calibration with a β-source

The detectors were calibrated in the LHC tunnel with a Sr-90 beta source, which provides electrons in the MIP energy range.

The response of one channel is shown in Figure 8 on a 10 ns/div time scale and a 5 mV/div amplitude scale in persistence mode as an example.

The average signal in Figure 9 demonstrates that there is no coherent noise in this measurement.

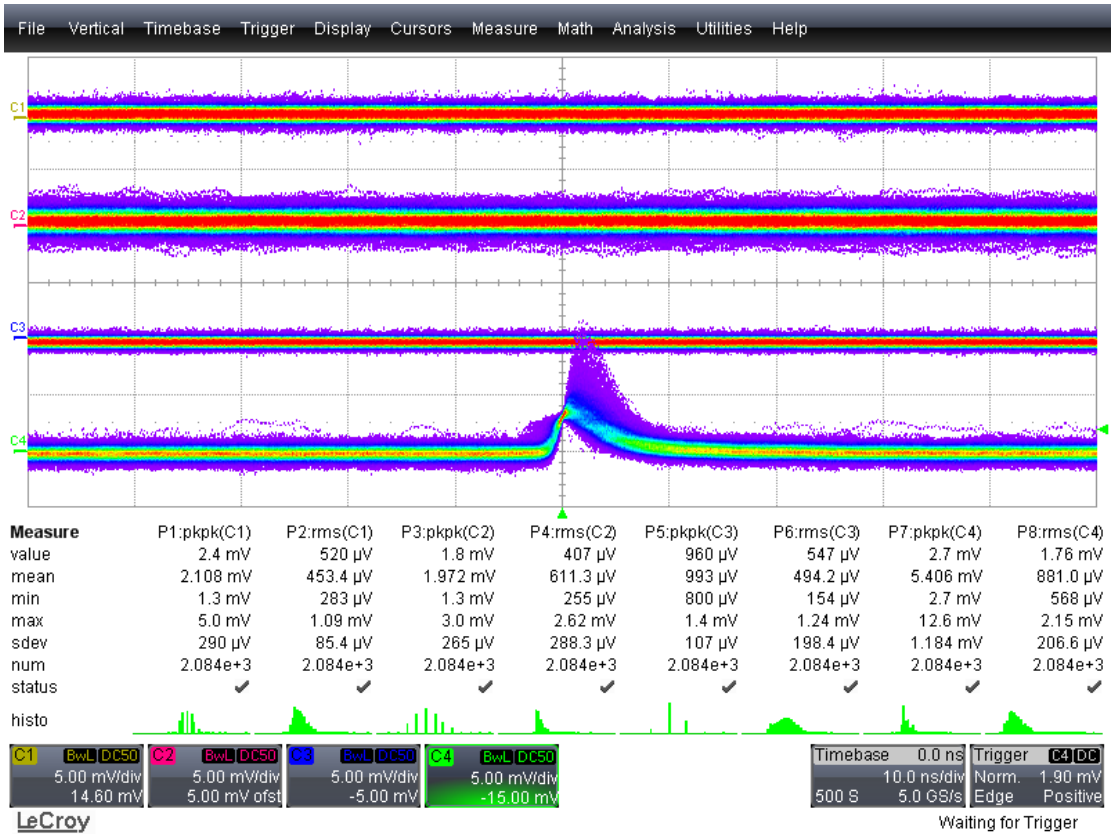

Figure 8: Persistence plot of calibration pulses from a Sr-90 beta source.

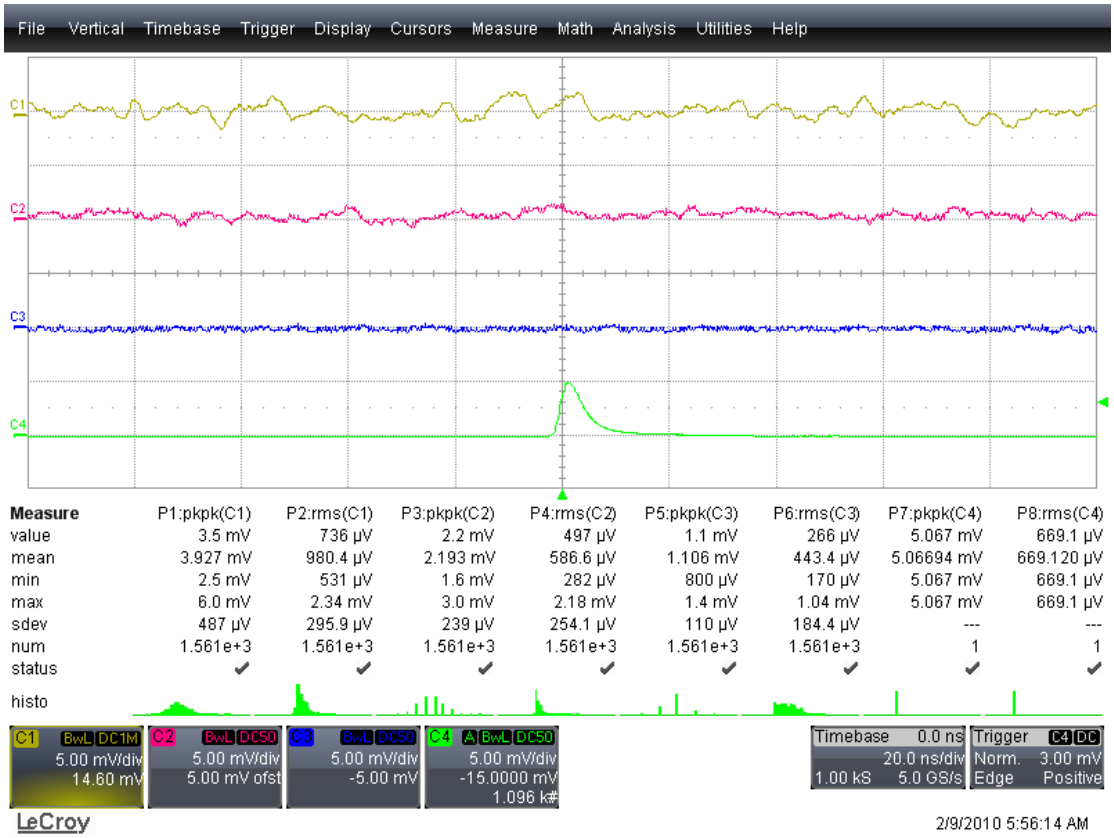

Figure 9: Calibration pulses in average mode. No coherent noise

can be observed.

3 Measurements

3.1 Pulses and their reconstruction

A Landau fitting procedure was used to reconstruct pulses. Figures 10 A-D show four examples for pulse reconstructions: A) single pulse, B) two separated pulses, C) double pulse and D) triple pulse.

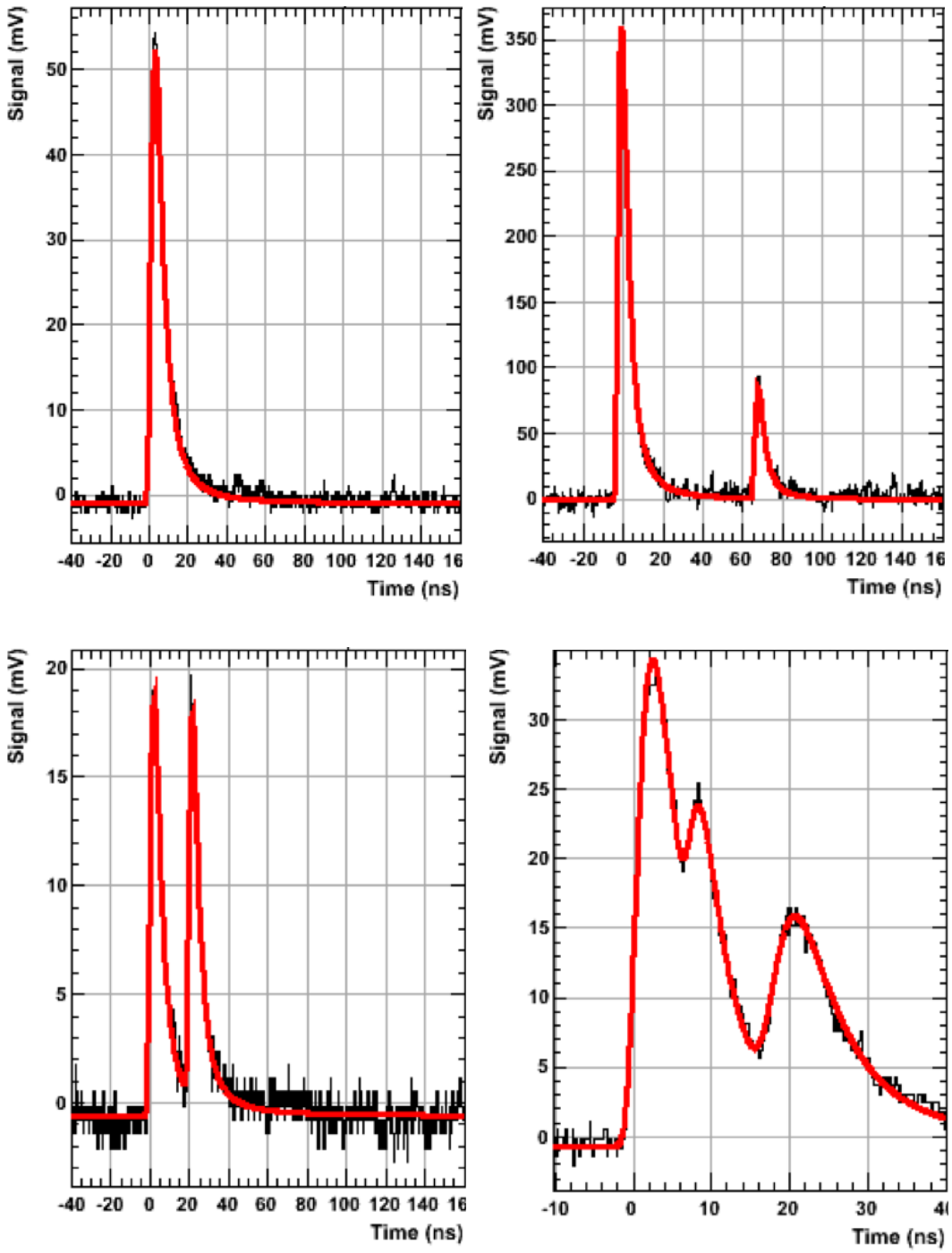

Figure 10: Four examples for pulse reconstruction: A) single pulse, B) two pulses, C) double pulse and D) triple pulse.

3.2 Recorded losses

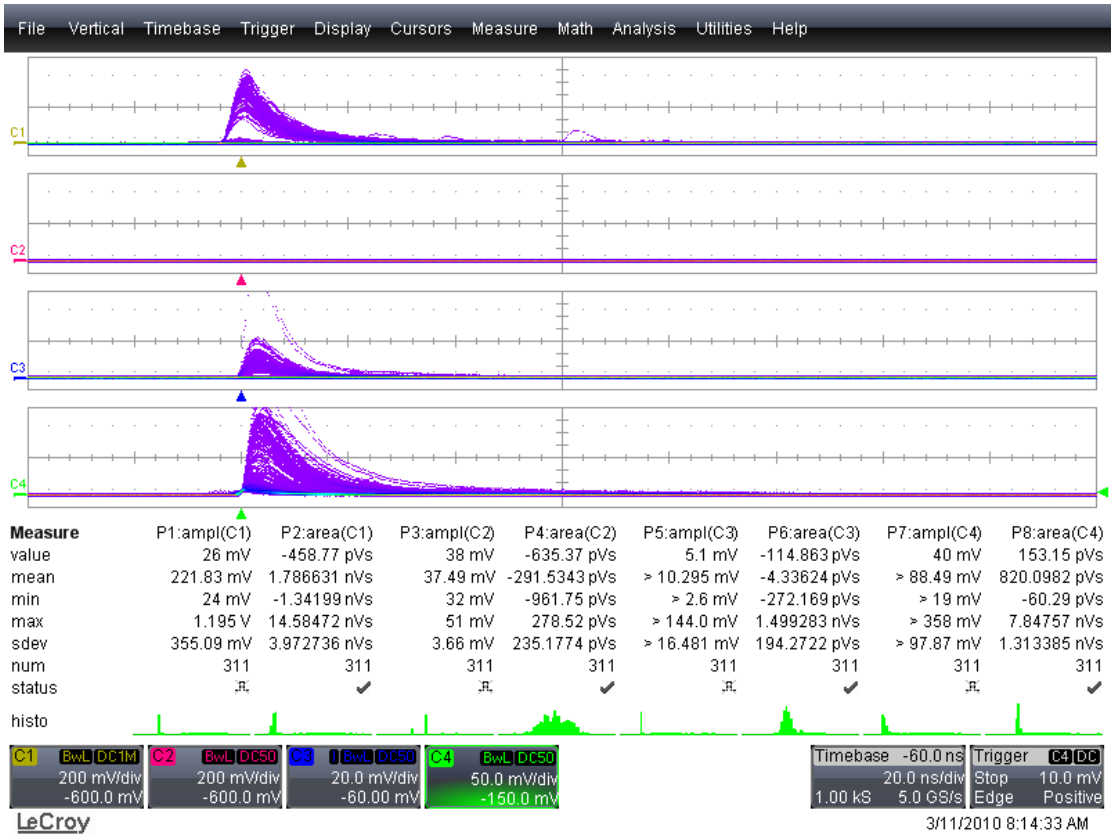

Figure 11: Pulses from the right channels C1, C2 and C3.

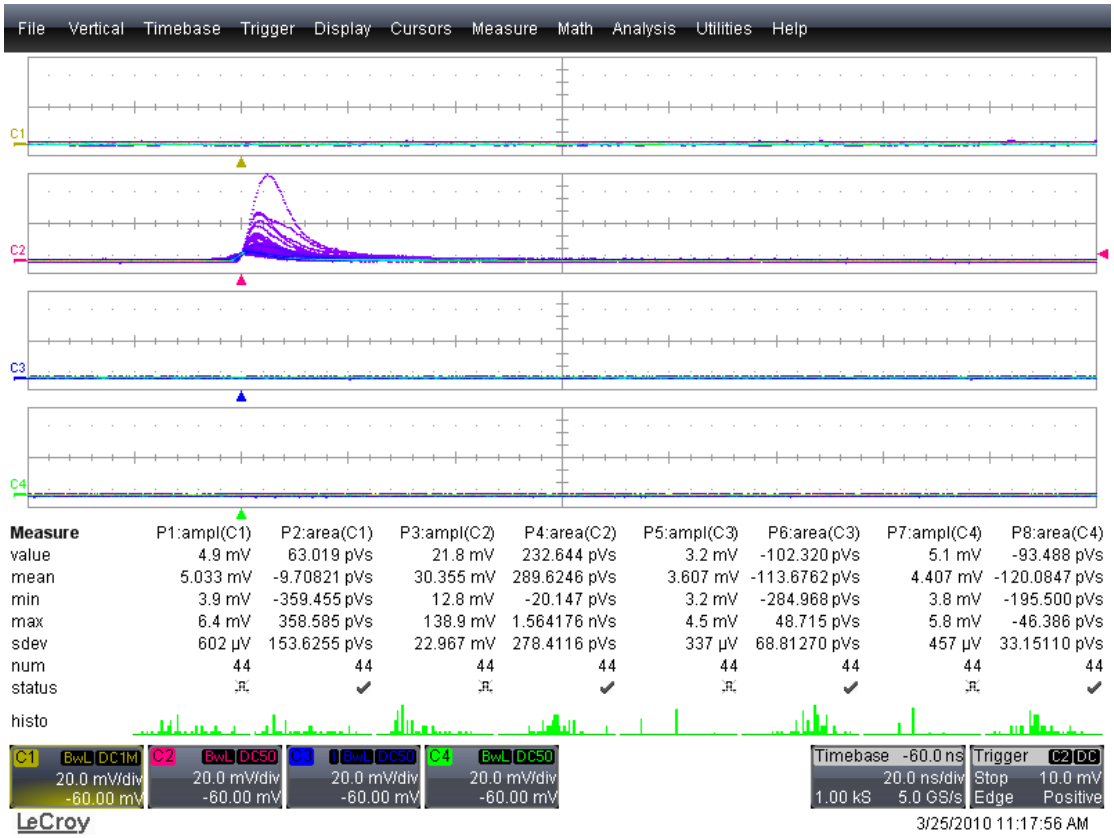

Figure 12: Pulses from the left channel C4.

3.3 Amplitude response

The amplitude histogram of pulse amplitudes and the baseline noise is given in the Figure 13. The noise has a sigma of 0.414 mV and the amplitude distribution shows a mean value of 16.859 mV and a maximum close to 100 mV.

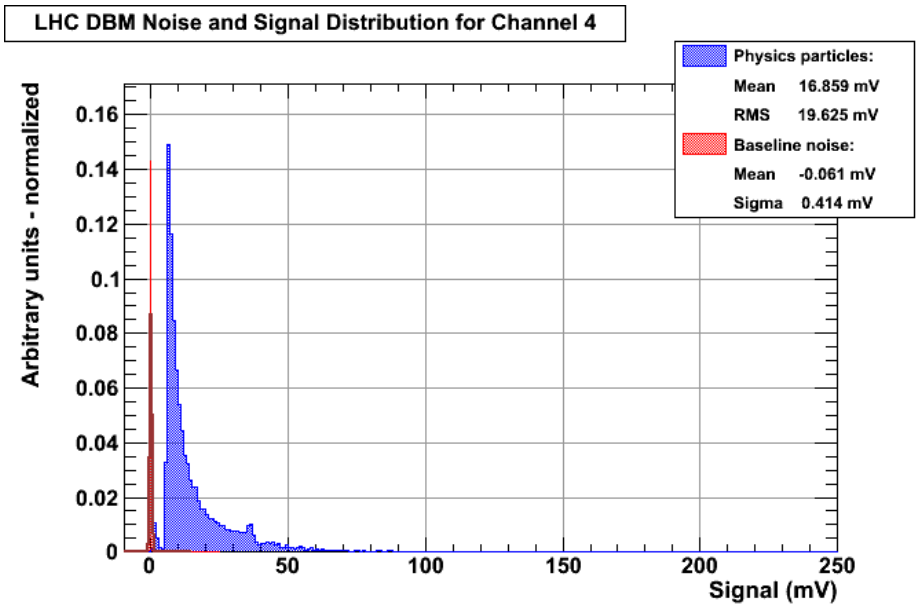

Figure 13: Example of the amplitude distribution in a reference channel.

3.4 Timing properties

Figure 14 shows the reconstructed timing properties of one channel. In this example the average rise time is 1.55 ns, the average fall time is 6.55 ns and the average pulse width is 6.18 ns.

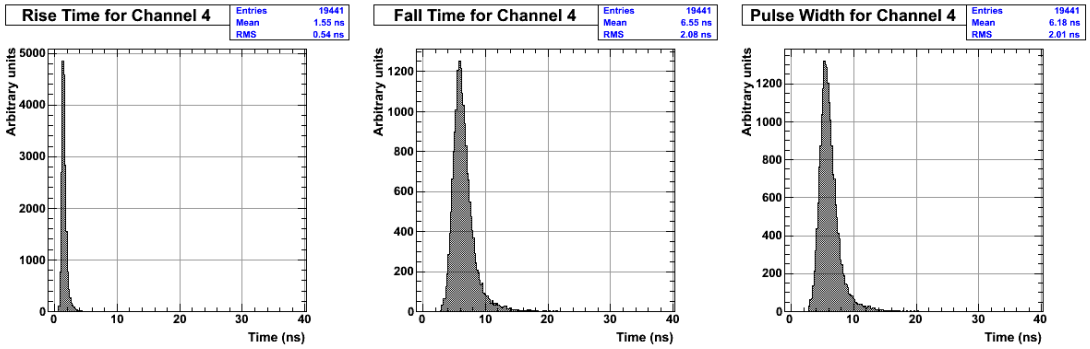

Figure 14: Timing properties of a reference channel.

Figure 15 shows the dependence of the timing parameters of the pulse amplitude, where the linearity of the amplitude response is demonstrated at high amplitudes. The correlation between rise time and fall time versus the pulse width gives a measure for the quality of the fit. In this example, Figure 16, a significant linear correlation between these parameters is demonstrated.

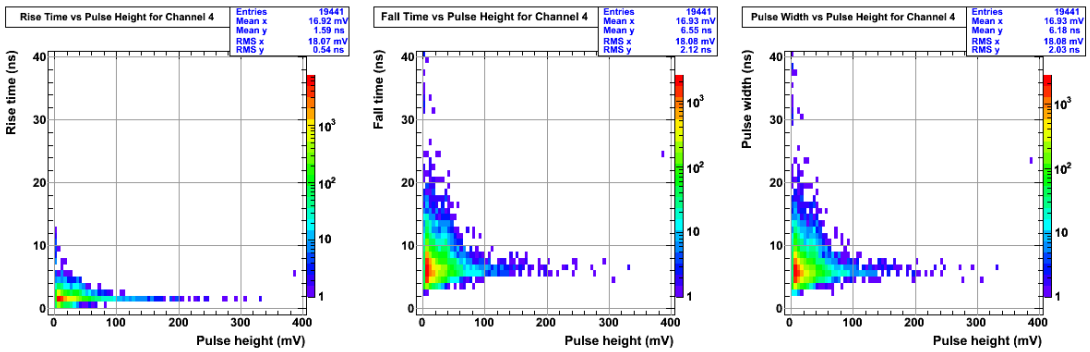

Figure 15: The dependence of the timing parameters of the pulse amplitude.

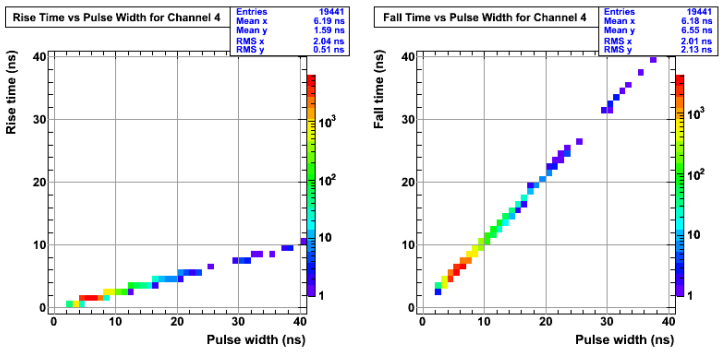

Figure 16: Linear correlation of the rise time and the fall time with the pulse width.

3.5 Time resolution

The time resolution of the DBLM has been determined by histogramming the difference in time response of two channels. The time response is evaluated at the FWHM of the pulses.

In Figure 17 the distribution is shown with 4757 entries. The sigma of the distribution represents the time resolution.

In this example the time resolution is 880 ps.

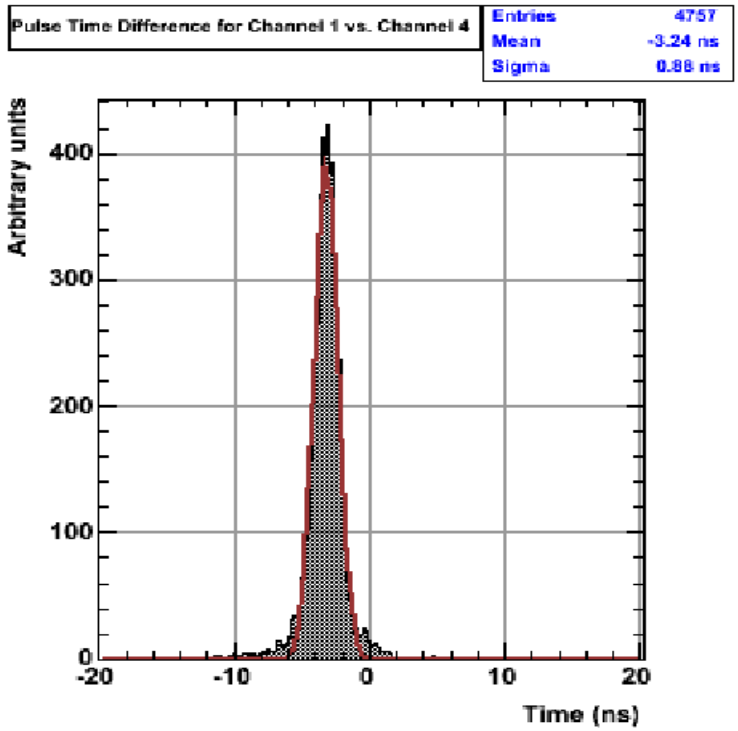

Figure 17: The time resolution of the DBLM is 880 ps.

3.6 Trigger efficiency

Two detectors (C1 and C2) with an active area of 8 mm × 8 mm are separated axially by 16 mm, Figure 18. This gives an opening angle of 26.57° which defines the acceptance of the two detectors.

Particles arriving within this angle will hit both detectors.

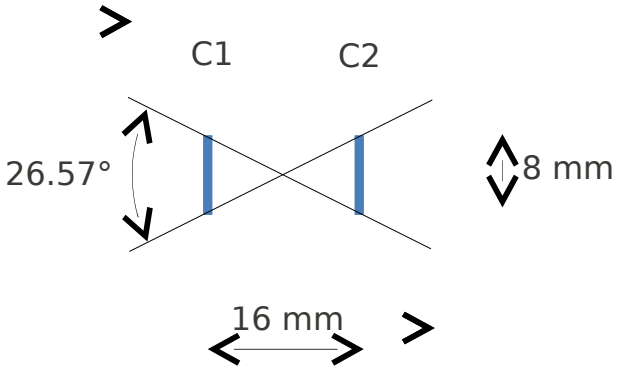

Figure 18: Alignment of two channels with an opening angle of 26.57°.

Three measurements were made to determine the efficiency of the detectors:

1. In the first measurement the detector C1 was the trigger channel and the coincidence with detector C2 was calculated to be 2.2%.

2. In the second measurement the detector C2 was the trigger channel and the coincidence with detector C1 was calculated to be 8.5%.

3. In the third measurement the detectors were tilted by 30° towards the beam. The detector 2 was the trigger channel and the coincidence with detector C1 was calculated to be 8.3%.

Run #	(C1 – C2) in %	(C2 - C1) in %	Remark
Waveform_ 24	2.2	97.2	Trigger on C1
Waveform_ 25	94.1	8.5	Trigger on C2
Waveform_ 26	94.4	8.3	Trigger on C2, detector tilted by 30°

We can summarize that:

1. No difference in efficiency can be observed with the tilted detector.

2. The efficiency is close to 100% for the non-triggered channel.

3.7 Phase measurement

The phase of the 40 MHz bunch crossing signal and a detector signal is shown in Figure 19. The 25 ns bunch spacing interval and the 2.5 ns RF period are shown in the diagram. The phase φ can be determined as the time difference between the FWHM of the signal and the bunch crossing signal (which is used as external trigger input and is not displayed), Figure 20.

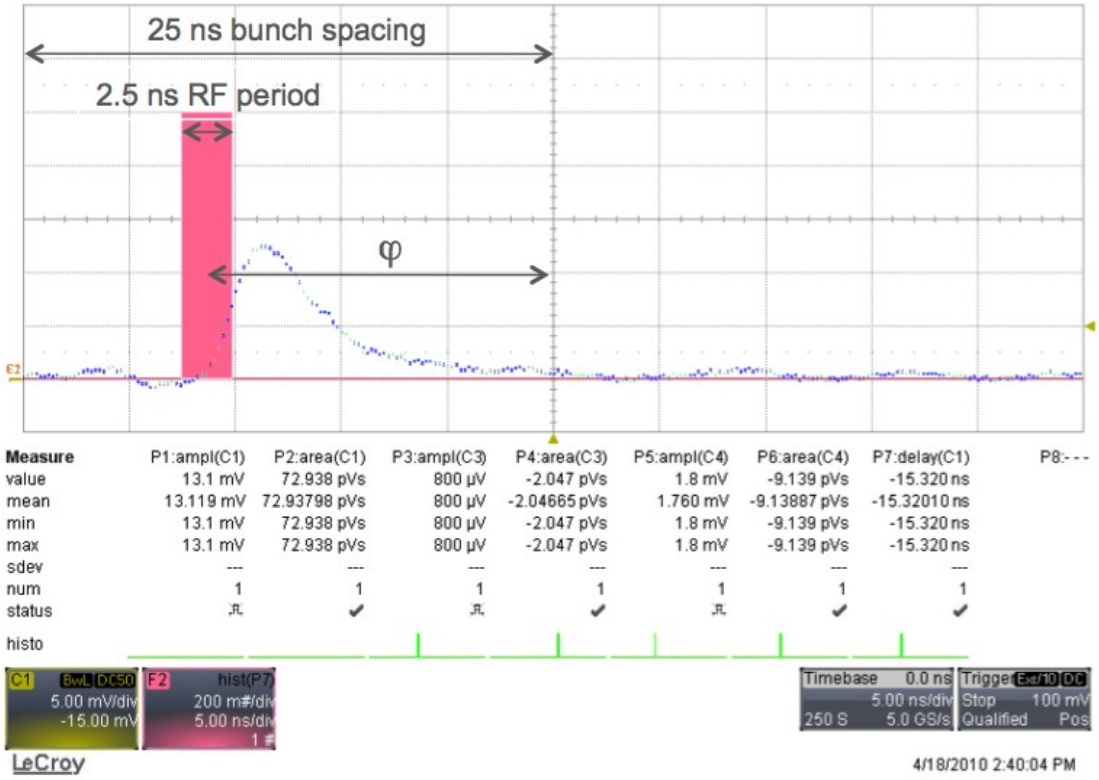

Figure 19: Phase measurement of the 40 MHz bunch crossing signal and a detector signal.

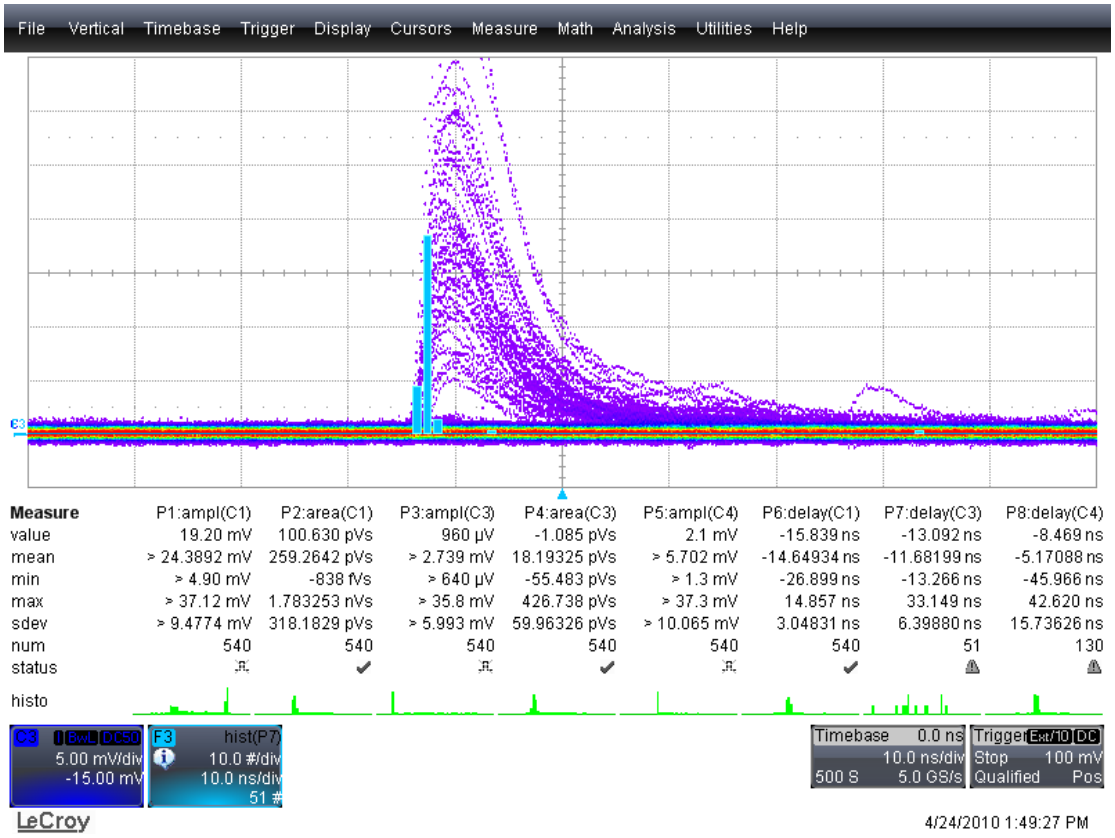

Figure 20: Phase distribution of the detector signals with respect to the 40 MHz bunch crossing signal of the LHC. The distribution shows a $\sigma = 3$ ns.

The phase distribution of Figure 20 shows a standard deviation $\sigma = 3.0$ ns.

3.8 Timing histogram

The LHC clock was used as a trigger signal in order to resolve the position of individual particle losses. These positions correlate with the bunch number in the machine.

The Figure 21 shows the LHC clock signal with a period of 89 us and the position of a single pulse. Figures 22-24 show some other examples.

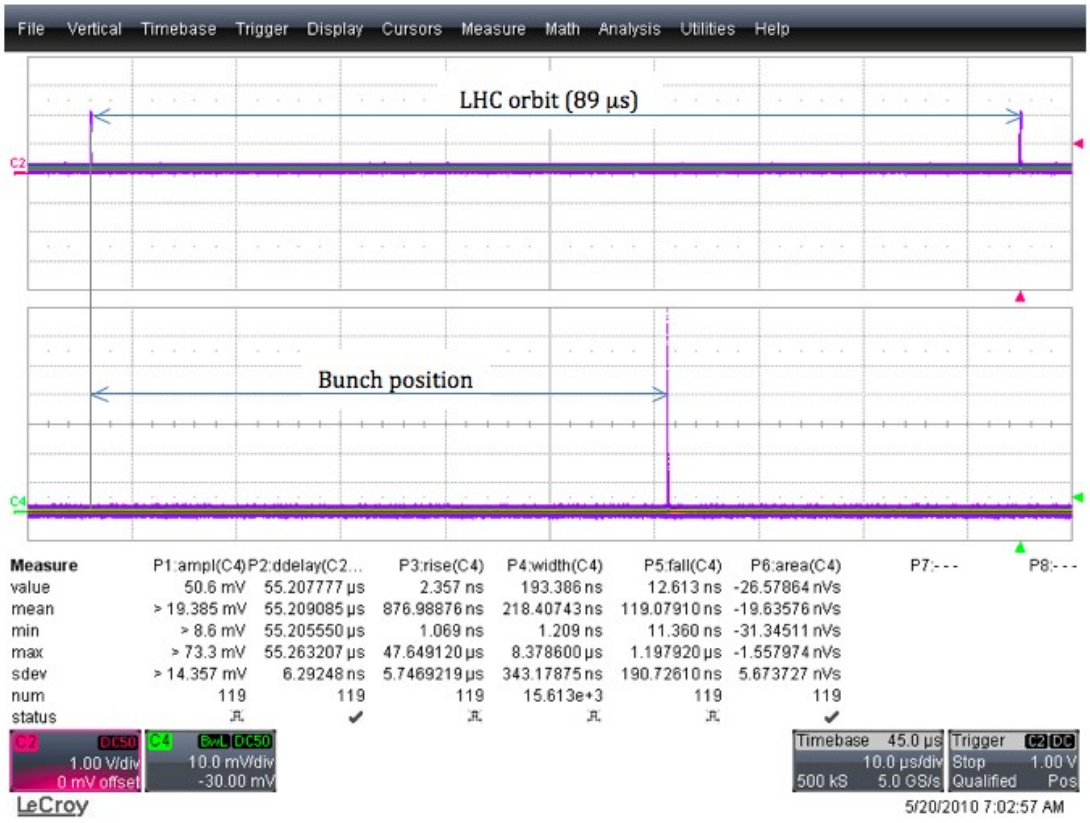

Figure 21: LHC clock and a single pulse.

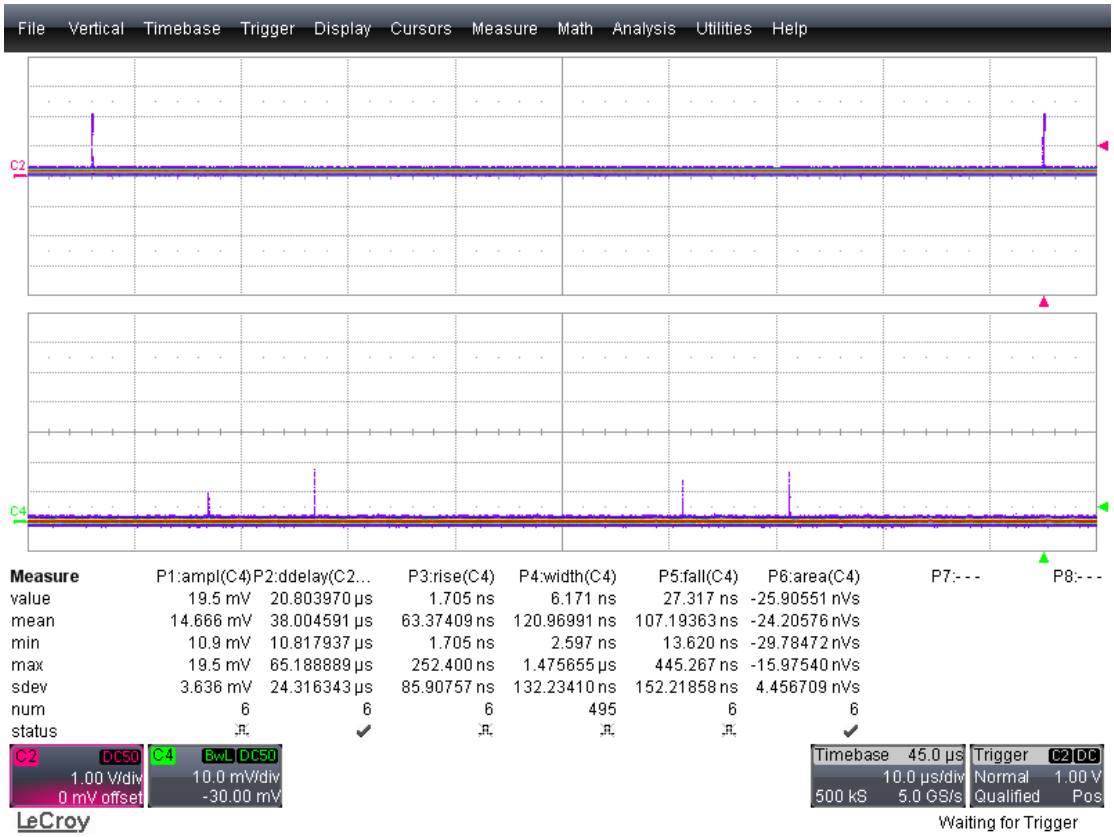

Figure 22: The LHC clock and four bunch locations.

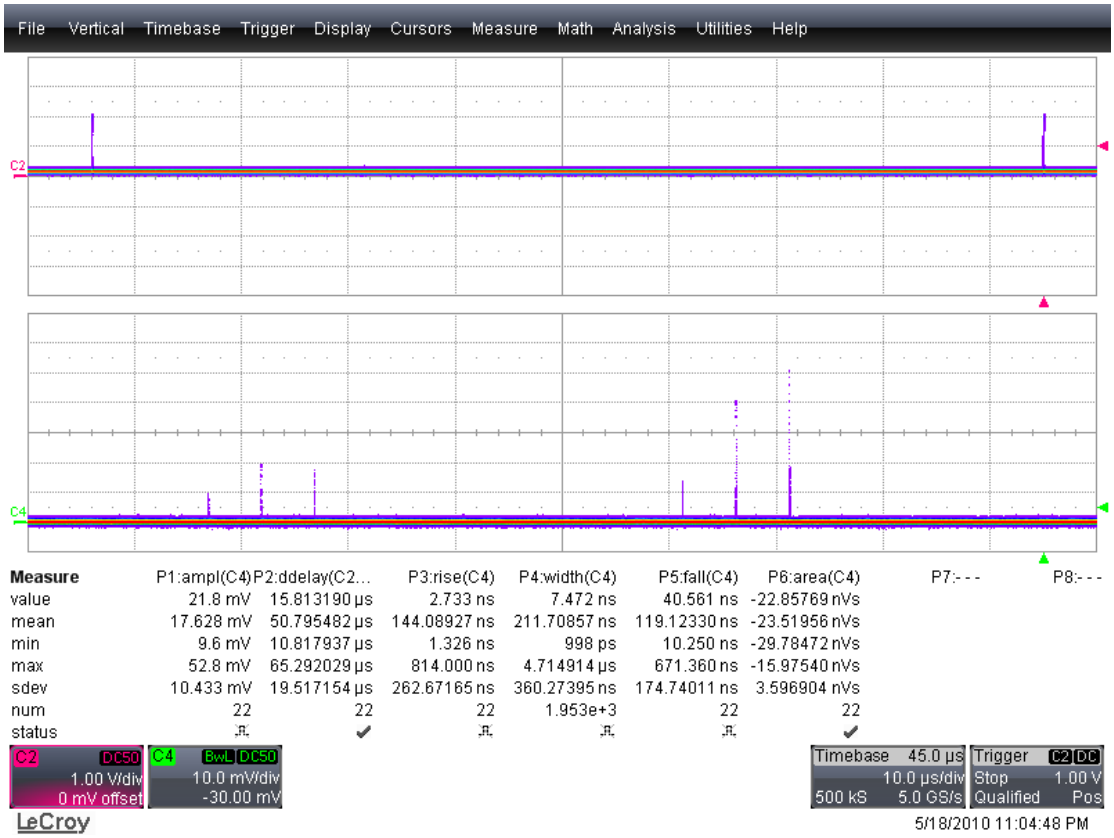

Figure 23: The LHC clock and 6 bunch locations.

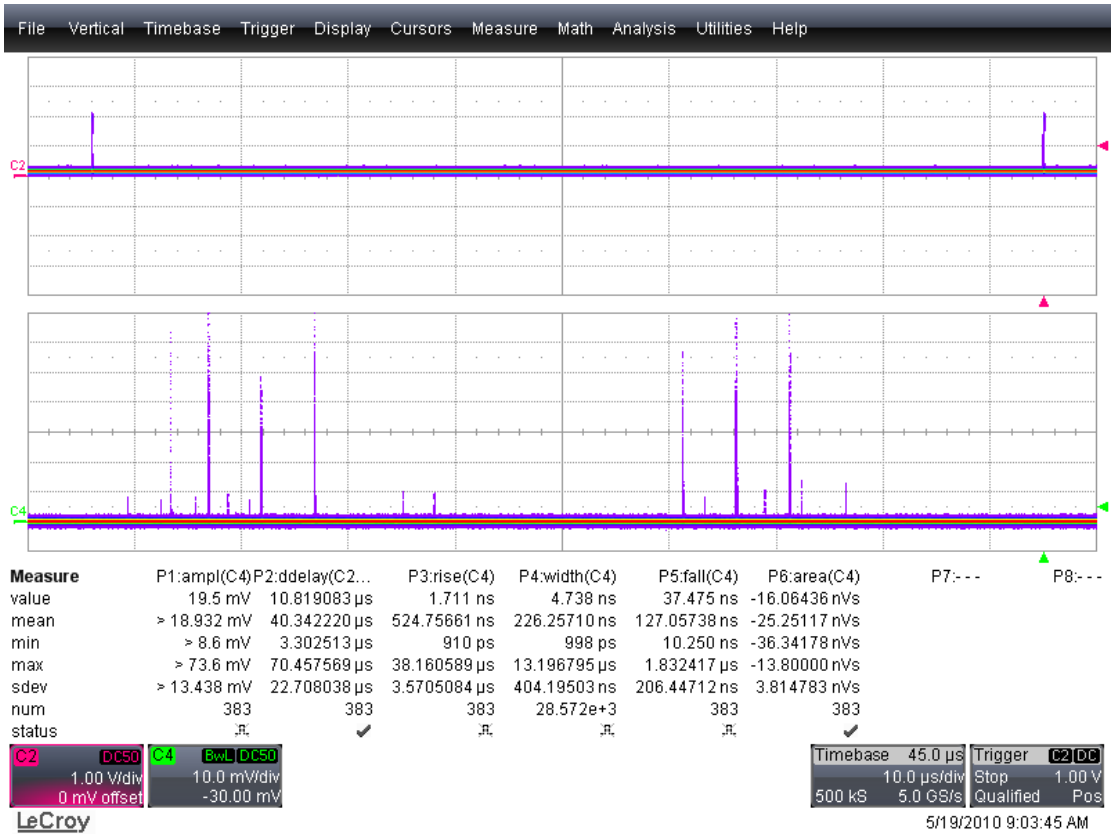

Figure 24: The LHC clock and six bunch locations with some ghost bunches.

4 Post mortem analysis

4.1 Example 1

Date: 3/10/2010 12h48, 152 bunches, 150 ns bunch spacing

In the following 6 figures (25-30), data of a beam abort event, taken with the Diamond Beam Loss Monitors, are shown. Starting with the buffer size of 10 ms, a zoom into the memory in five stages is provided (corresponding to time scales from 1 ms/div, 100 us/div, 10 us/div, 1 us/div, 100 ns/div and 10 ns/div).

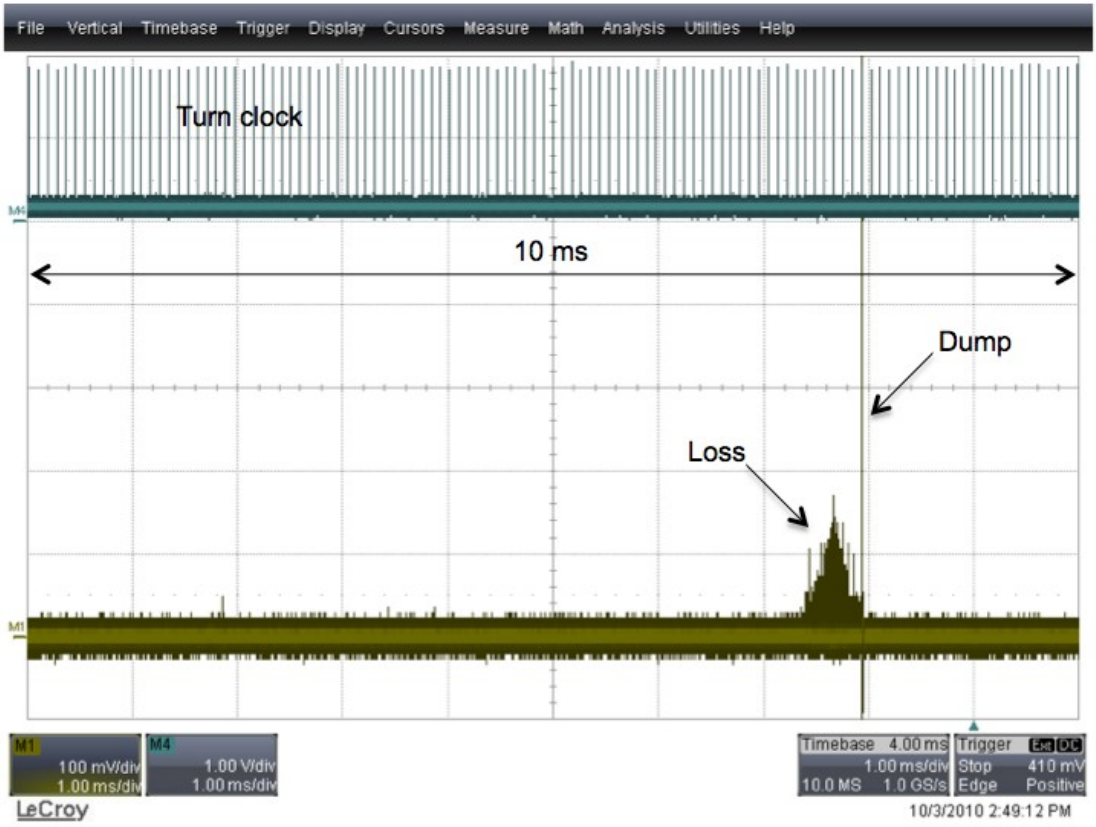

Figure 25: The 10 ms buffer (1 ms/div) shows the characteristics of the event and the turn-clock signal of LHC (89.2 us). The dump causes a high pulse at the end of the loss pattern.

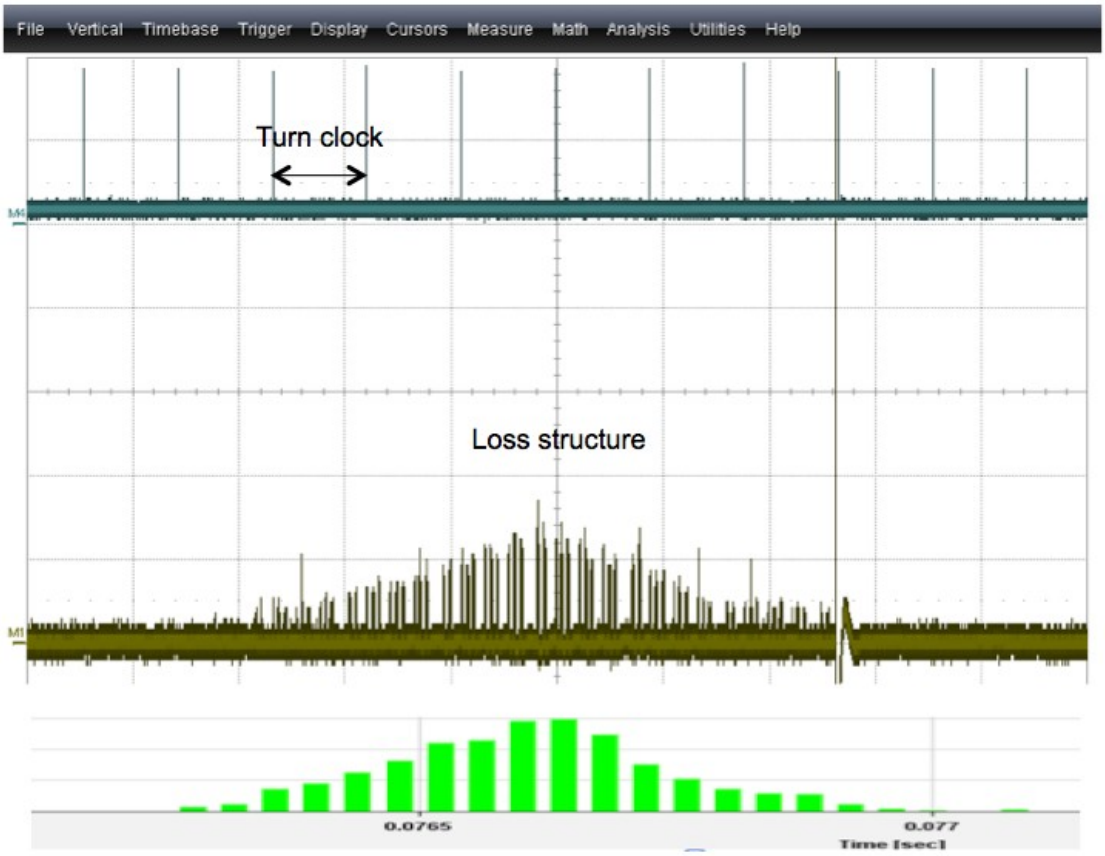

Figure 26: Zoom factor 10^1 (100 us/div): the time structure of the bunch trains can be estimated. The corresponding measurement from the ionization chambers is shown at the bottom and shows an excellent agreement between the DBLM and the ionization chambers.

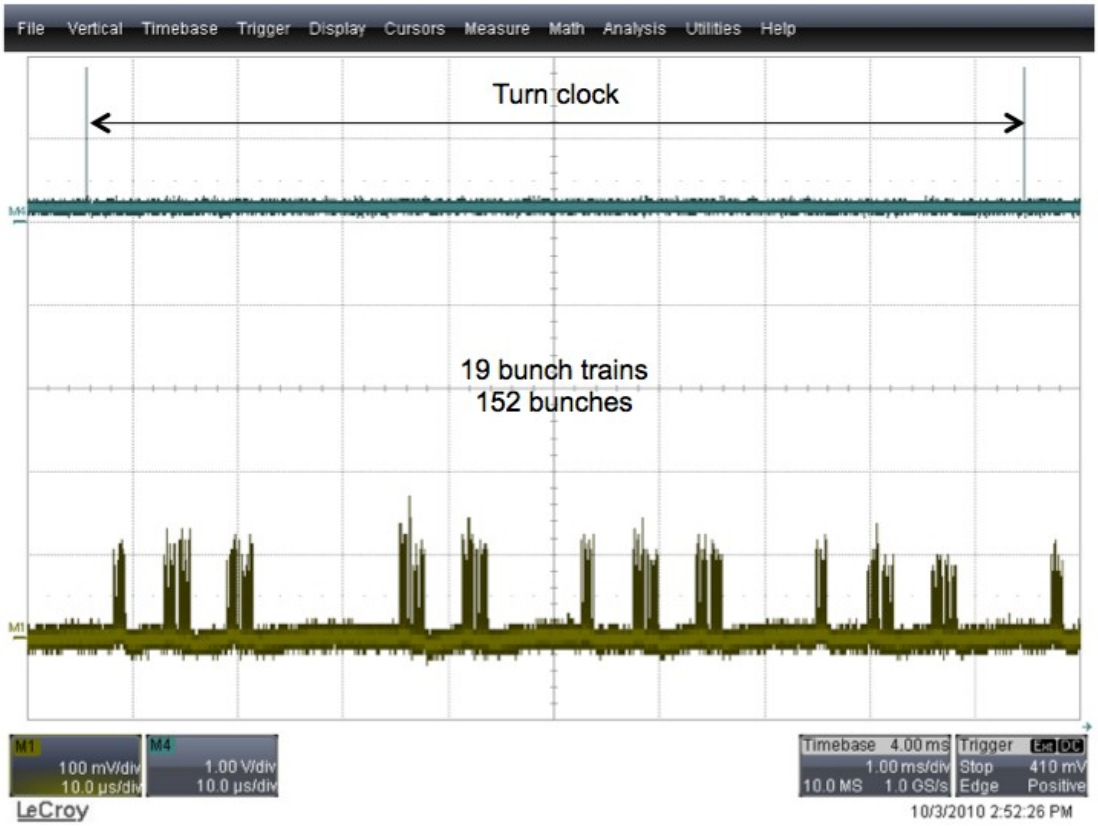

Figure 27: Zoom factor 10^2 (10 us/div): The bunch-train structure shows 8x16 and 3x8 bunch trains, corresponding to 152 bunches.

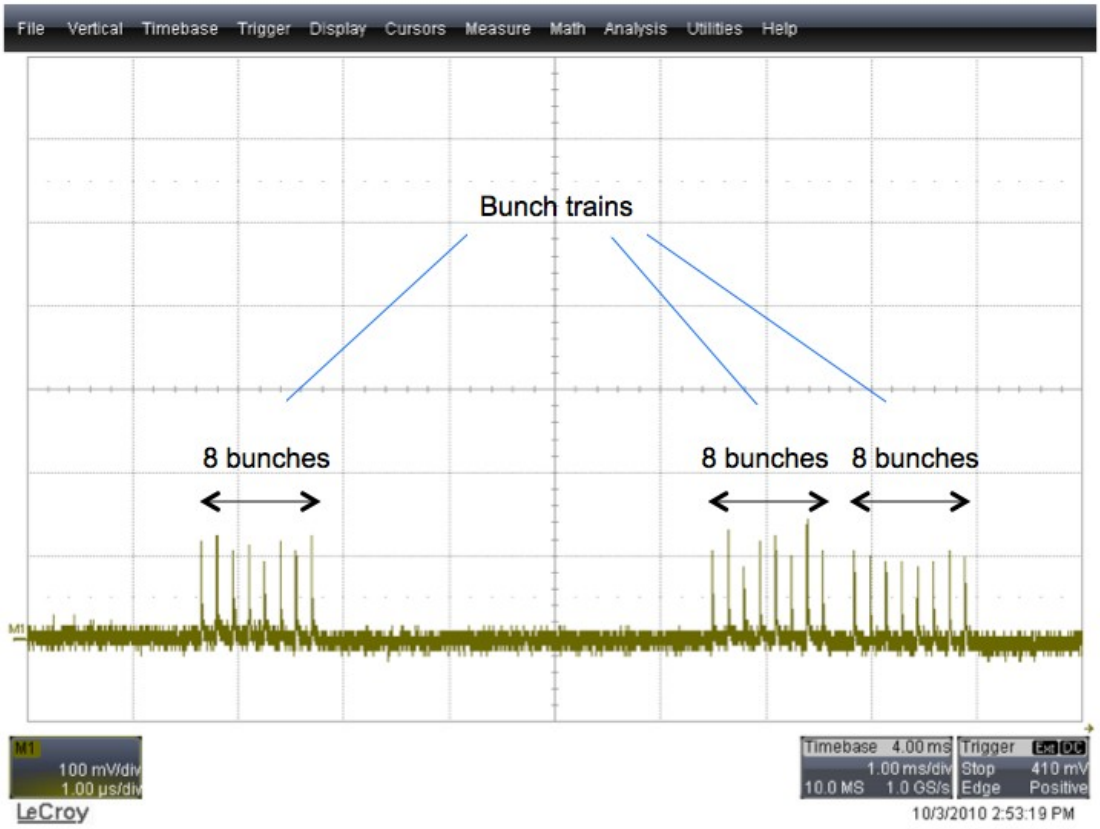

Figure 28: Zoom 10^3 (1 us/div): The bunch-train structure shows 8 bunches per bunch train. On the left side there is one train and on the right side there are two consecutive trains.

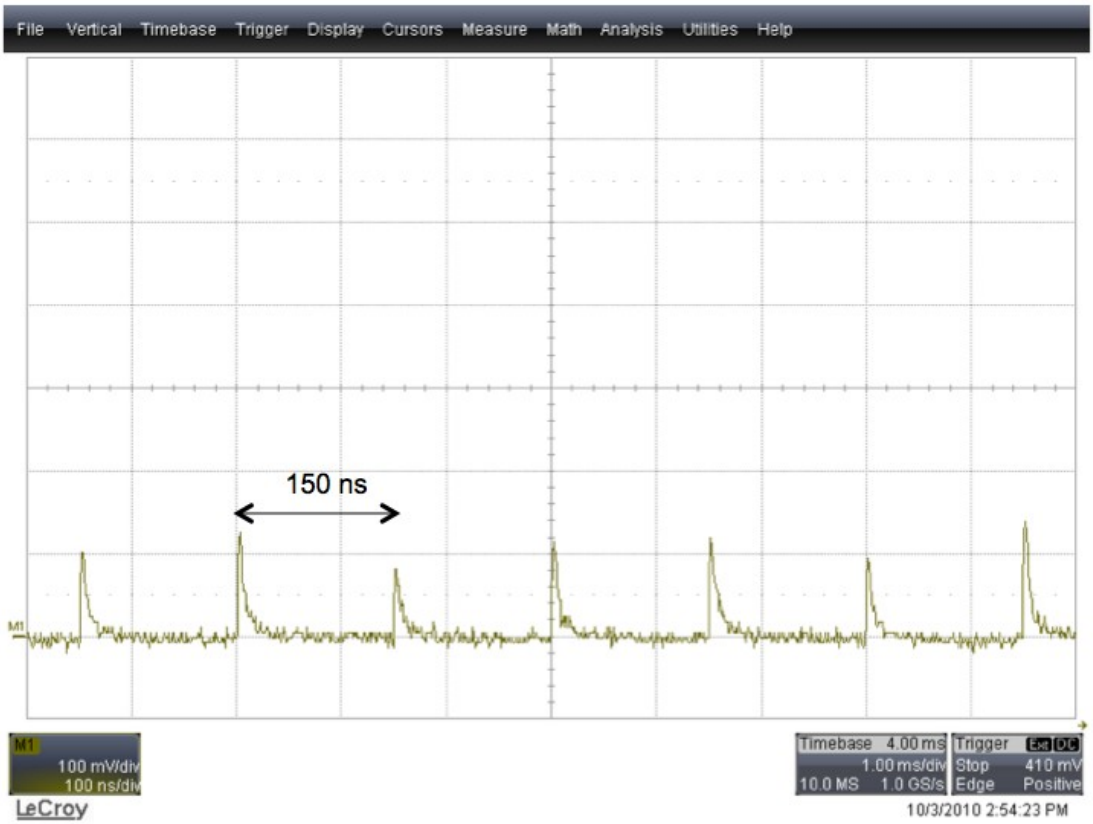

Figure 29: Zoom 10^4 (100 ns/div): Bunches are separated by 150 ns.

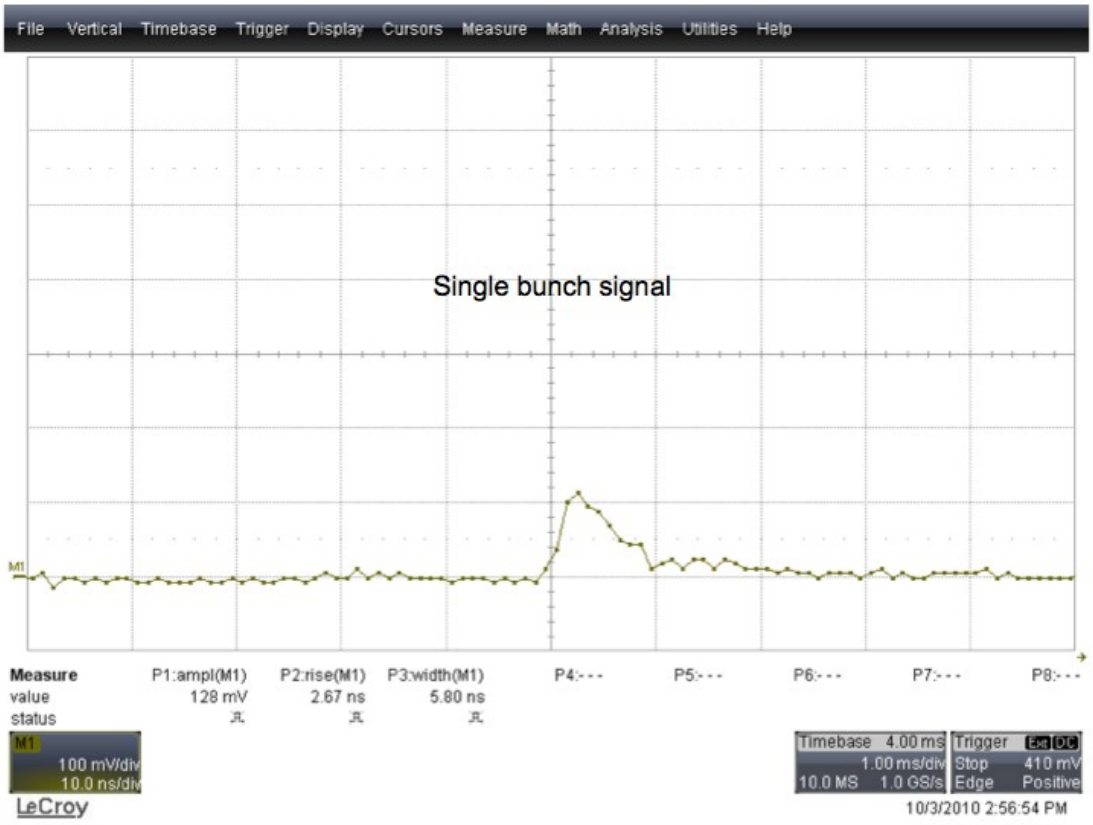

Figure 30: Zoom 10^5 (10 ns/div): A single bunch signal with an amplitude of 128 mV, a rise time of 2.67 ns and a pulse width of 5.80 ns. The amplitude corresponds to some 50 particles hitting the detector simultaneously.

4.2 Example 2

Figures 31-34 analyse another unscheduled beam abort. Date: 18/8/2010, 21h14

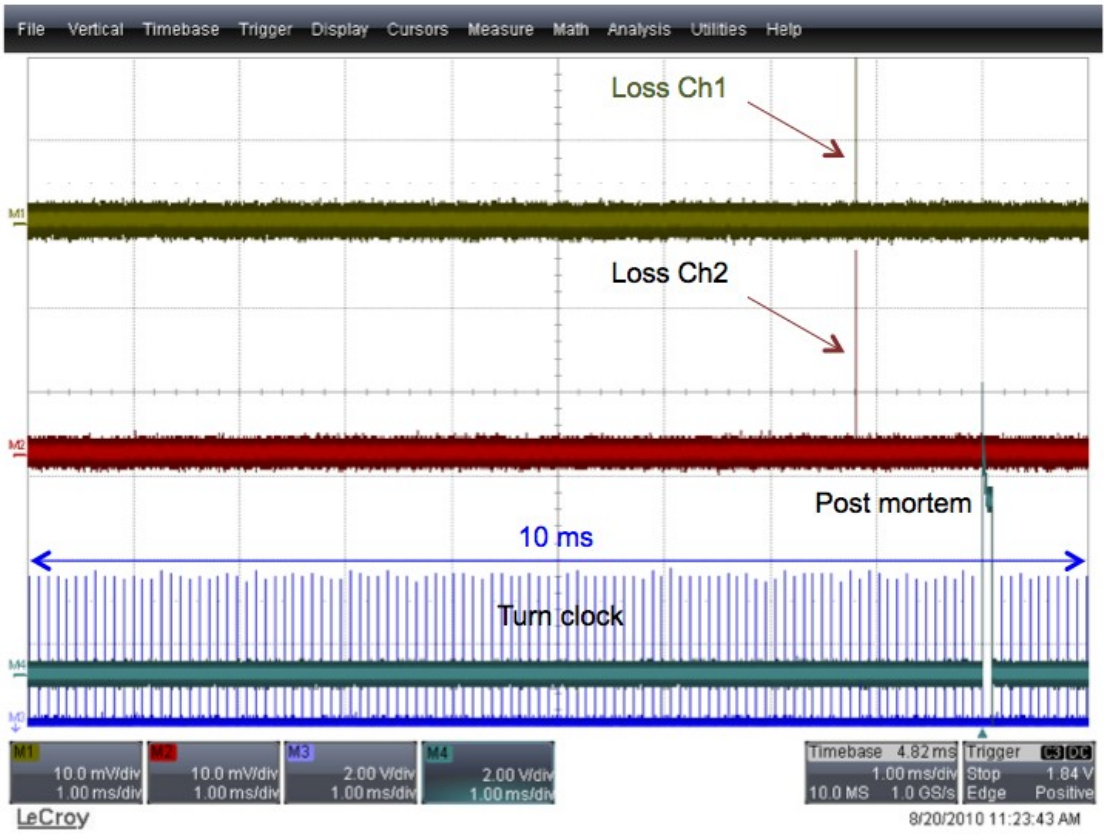

Figure 31: The above screen covers 10 million measurement points. One pixel on the screen averages over 10 thousand individual measurements. The buffer size is 10 ms and losses can be observed as two narrow pulses on two measurements channels.

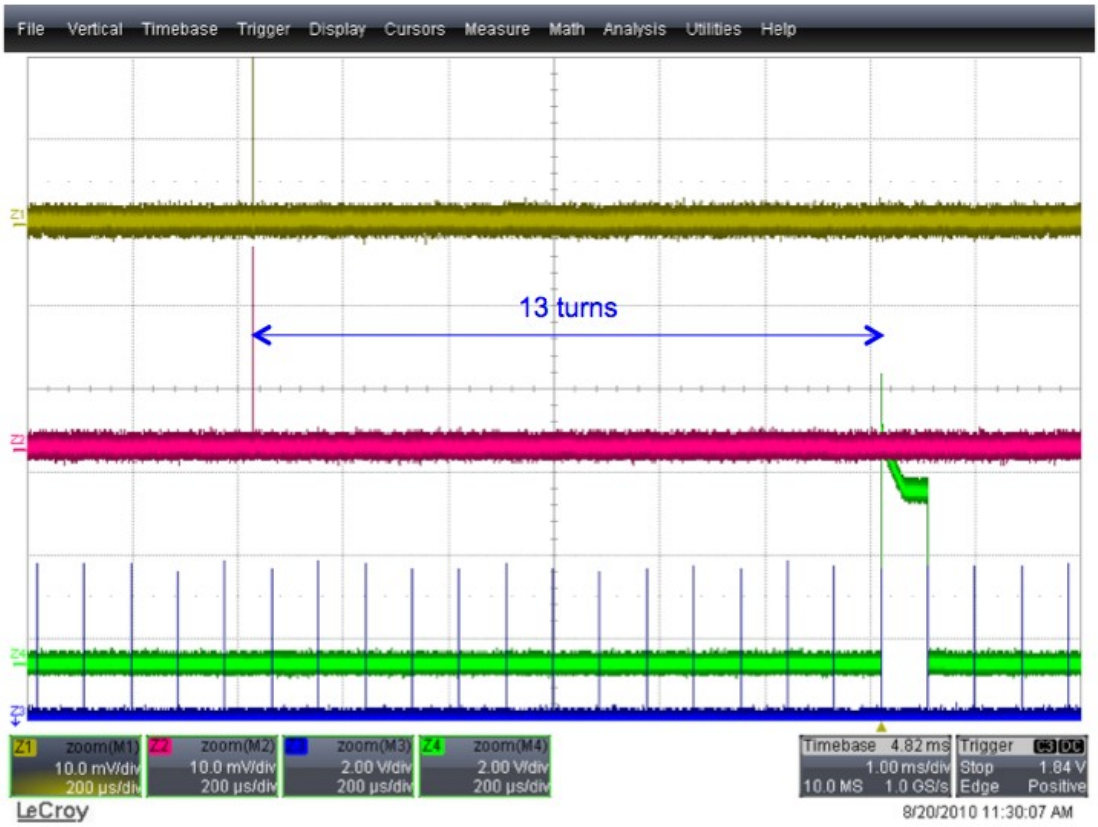

Figure 32: Two losses occur 13 turns before the post mortem signal appears.

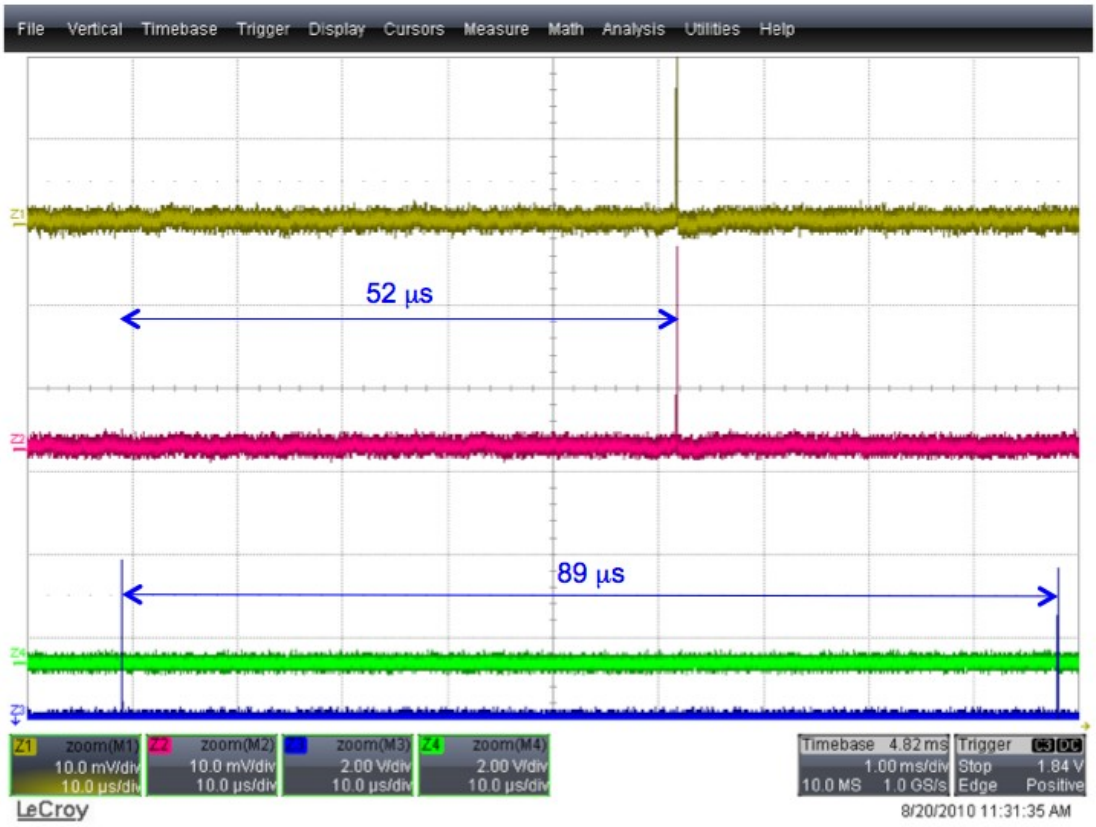

Figure 33: The phase of the losses relative to the LHC period.

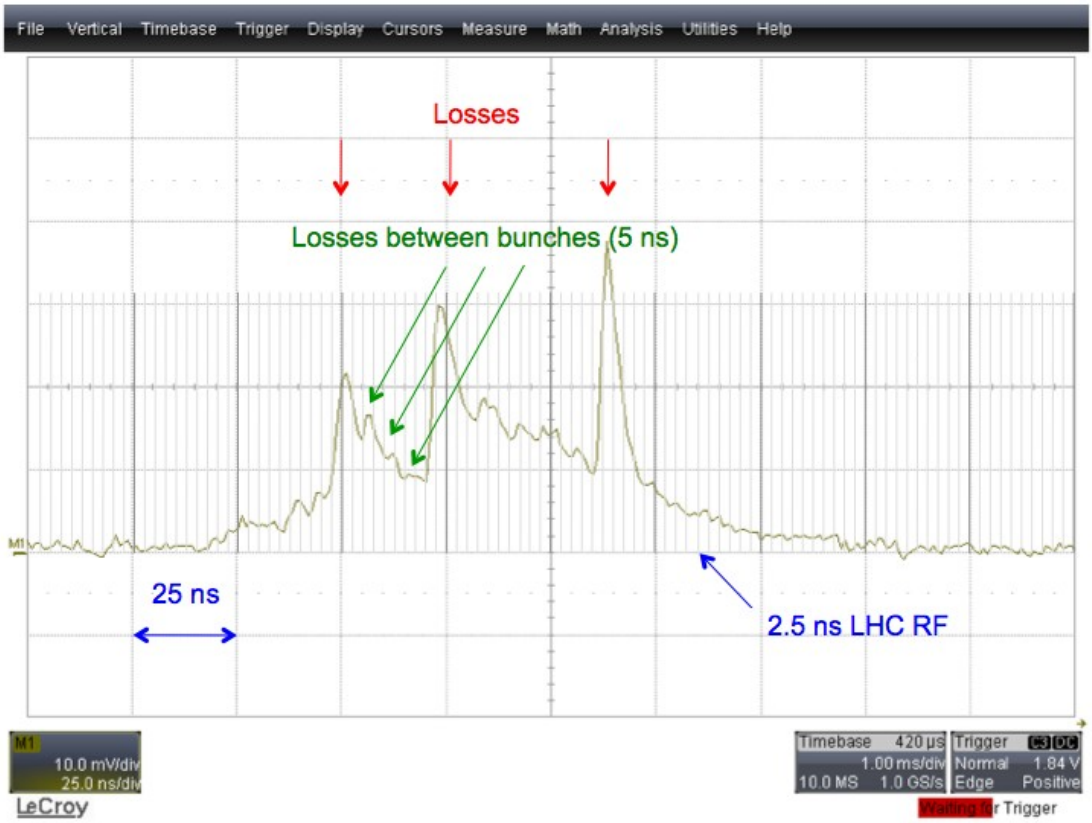

Figure 34: Beam loss profile. Two losses are in step and the third is out of step. Losses occurring between two bunches correspond to the SPS RF. The detector time resolution is below 1 ns.

4.3 Example 3

Figures 35-39 analyse another unscheduled beam abort. Date: 26/8/2010, 17h25

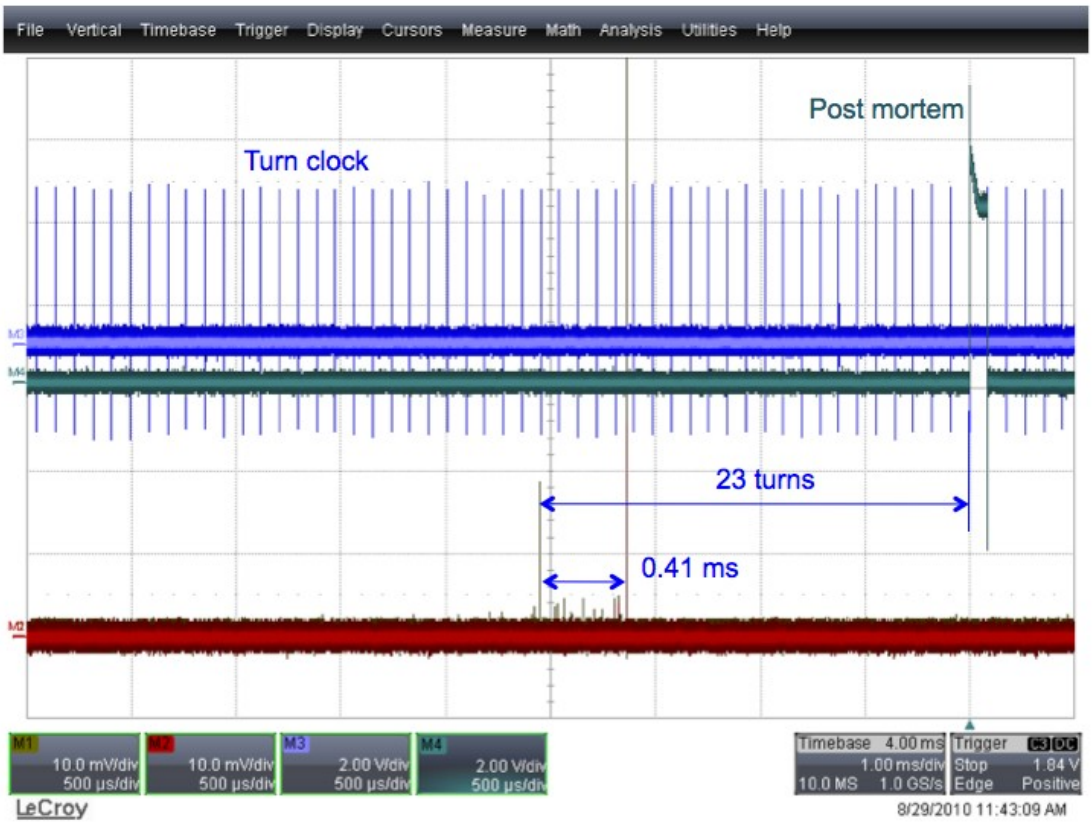

Figure 35: Beam loss profile of a post mortem event. The losses extend over 0.41 ms before the beam is dumped.

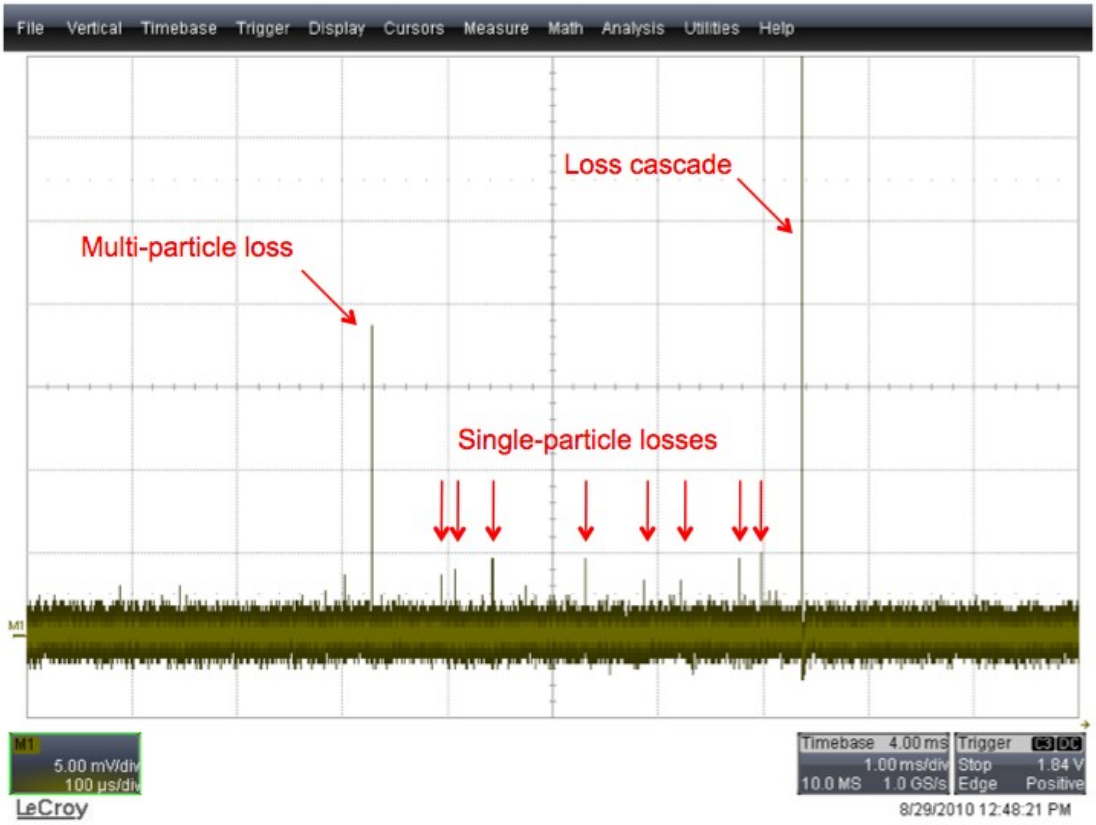

Figure 36: The beam loss profile shows multi-particle losses, single-particle losses and a loss cascade before the beam dump.

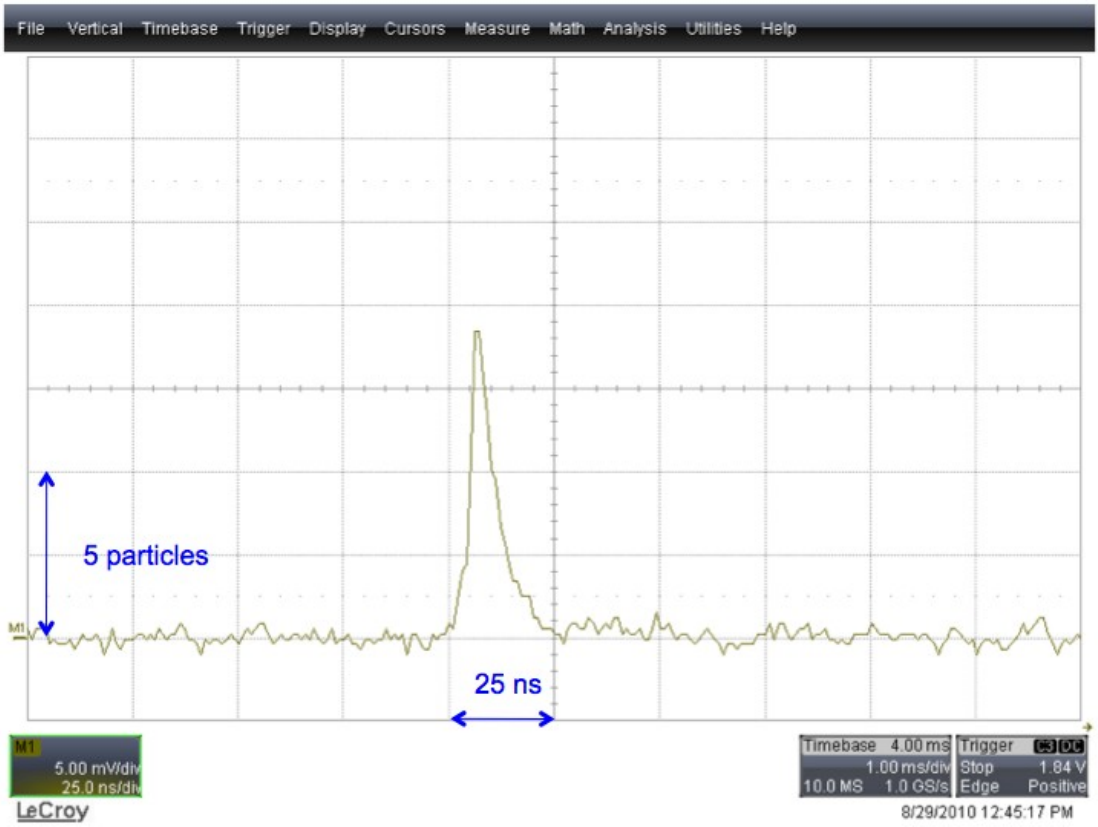

Figure 37: Multi-particle loss with an amplitude of 18 mV.

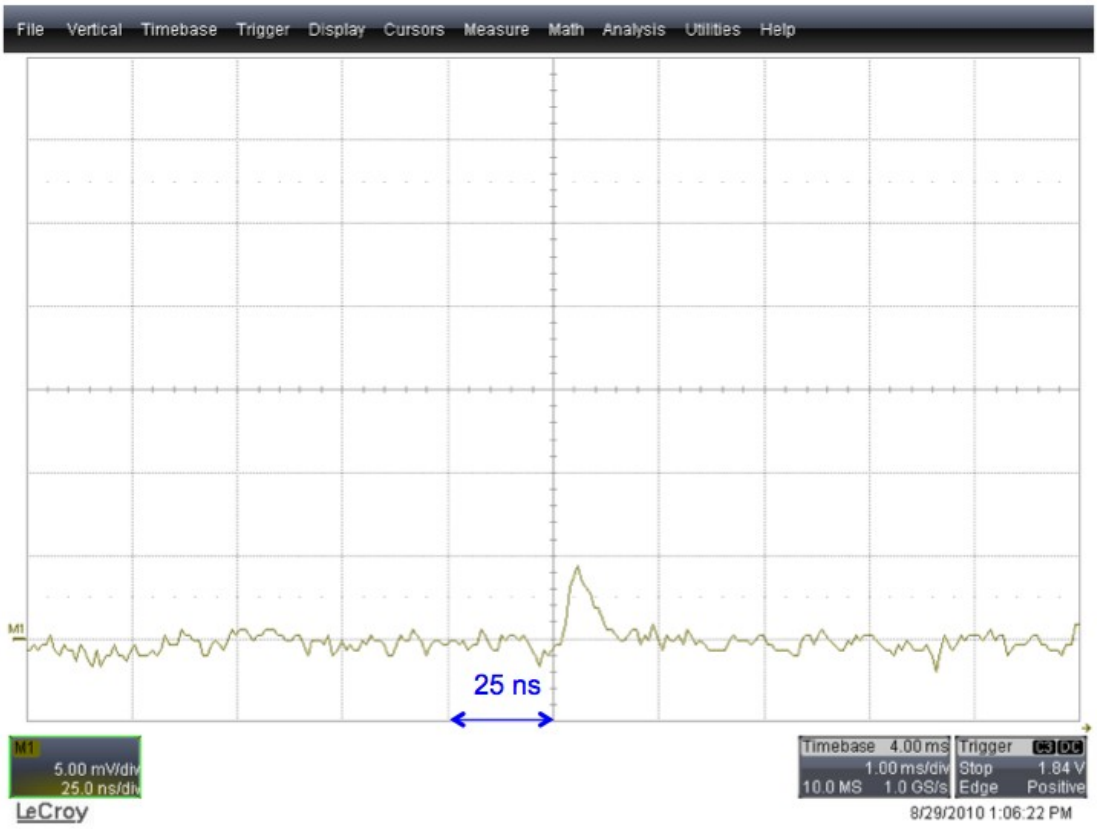

Figure 38: Single-particle loss with an amplitude of 4 mV.

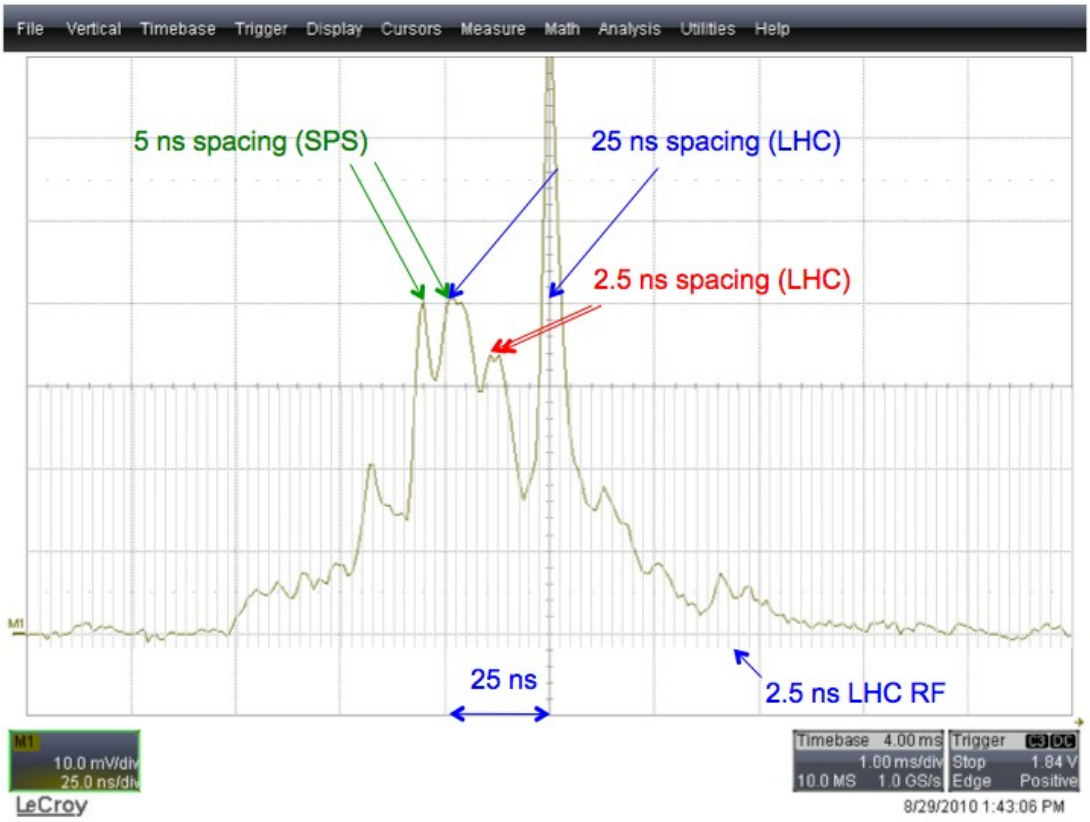

Figure 39: Loss profile before the beam is dumped. The RF time structure of the LHC (2.5 ns) and the SPS (4 ns) can be resolved by the diamond detector.

4.4 Example 4

Figures 40-43 analyse another unscheduled beam abort. Date: 22/9/2010 12h48, 24 bunches, 150 ns bunch spacing

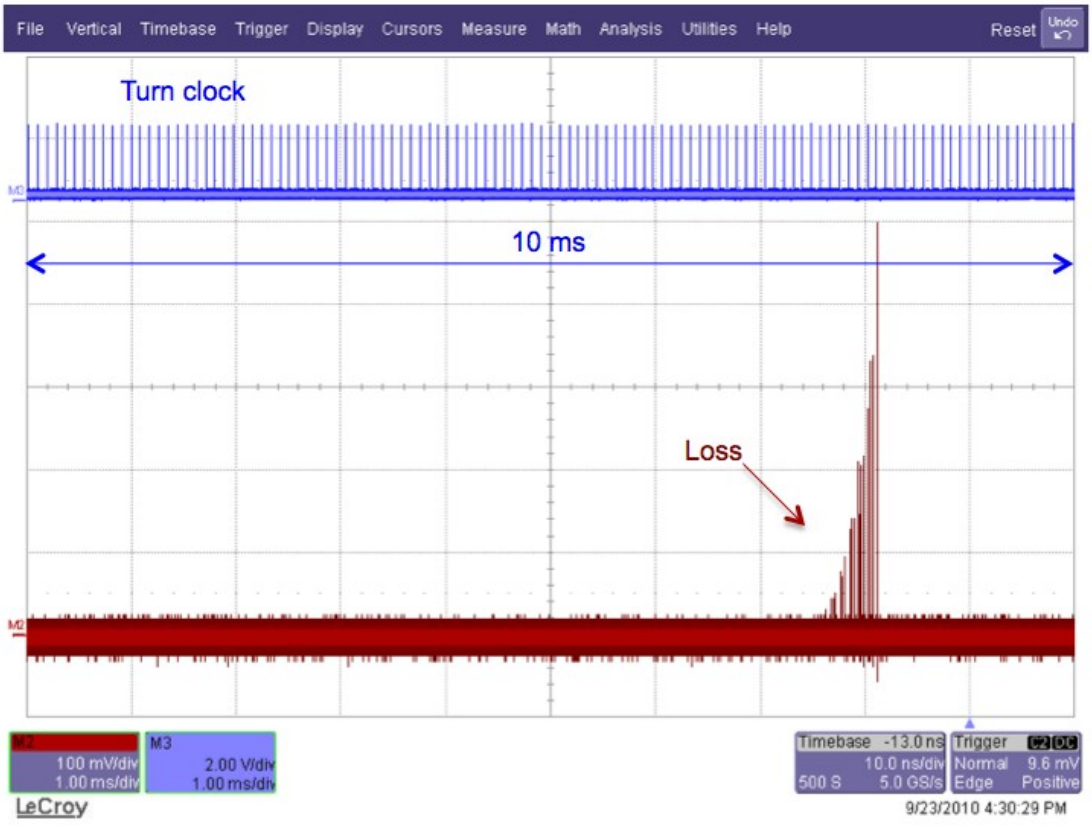

Figure 40: Beam loss profile with an exponential behavior. The time of the beam abort is indicated as pink trigger marker on the horizontal axis.

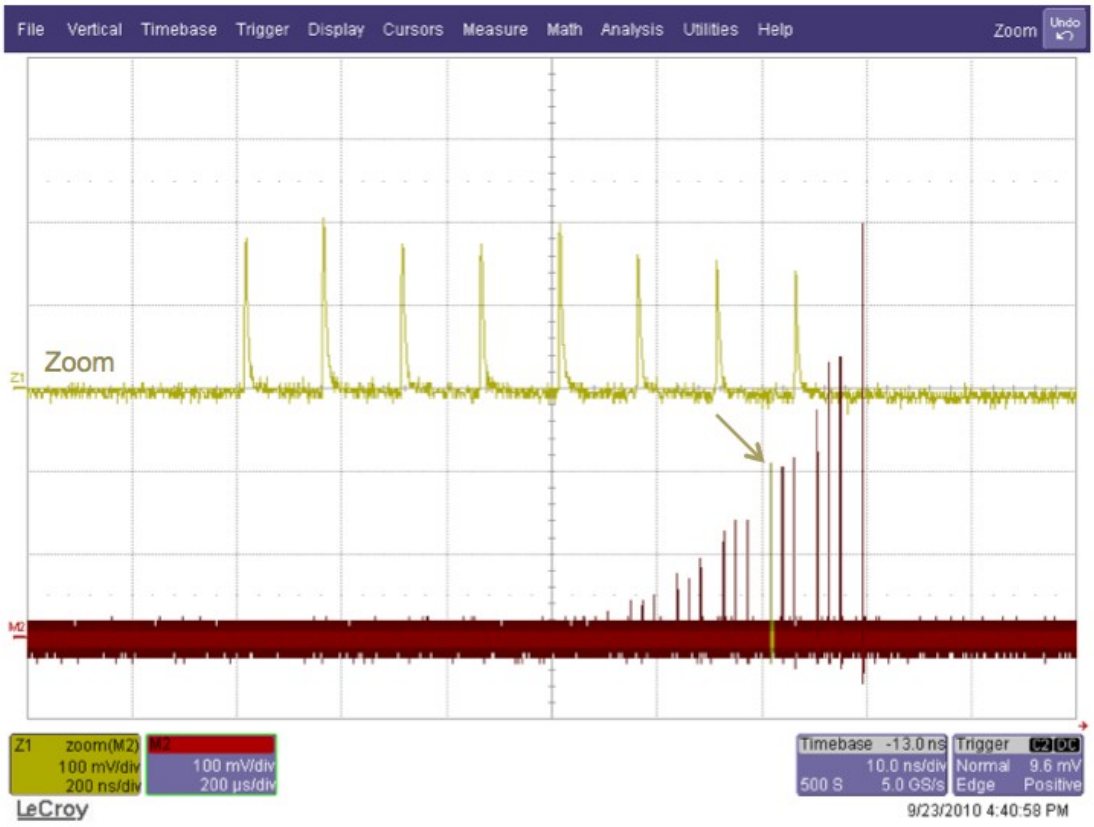

Figure 41: Each of the pulses (red) represents a bunch train with 8 bunches (yellow). The 8 individual pulses have similar amplitudes of the order of 200 mV, which indicates equivalent losses inside the bunch trains.

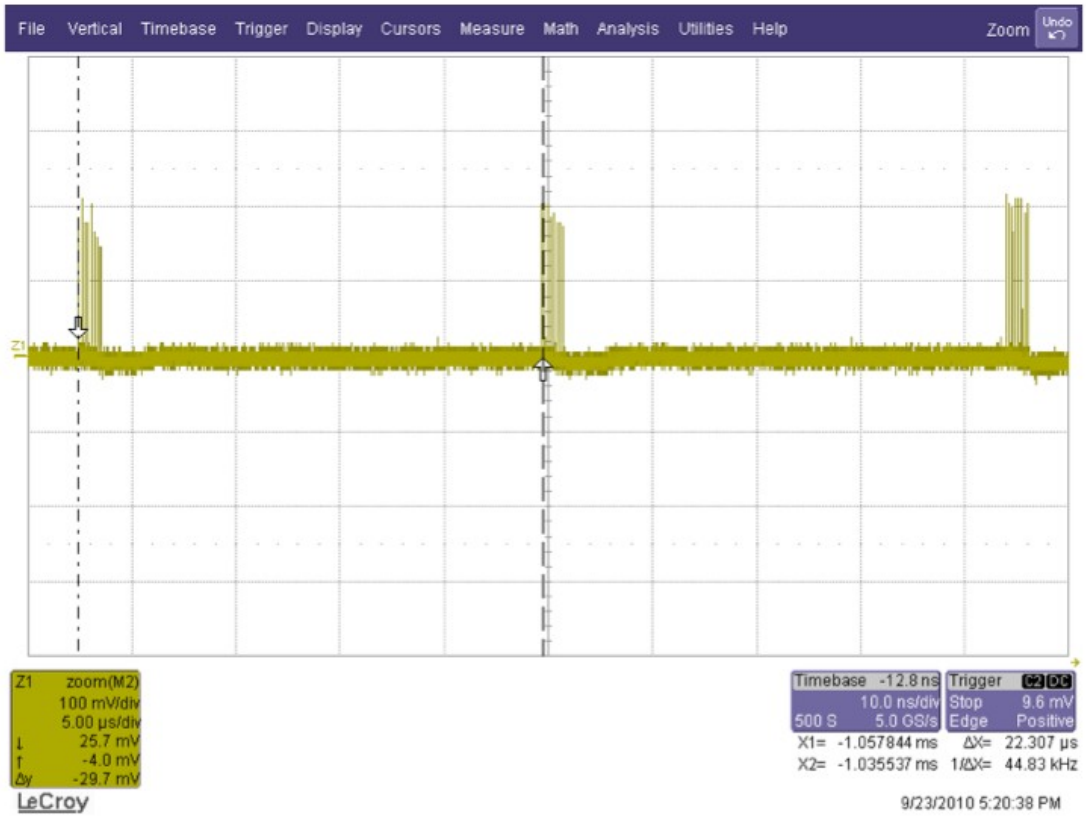

Figure 42: The bunch trains are separated by 22.3 us.

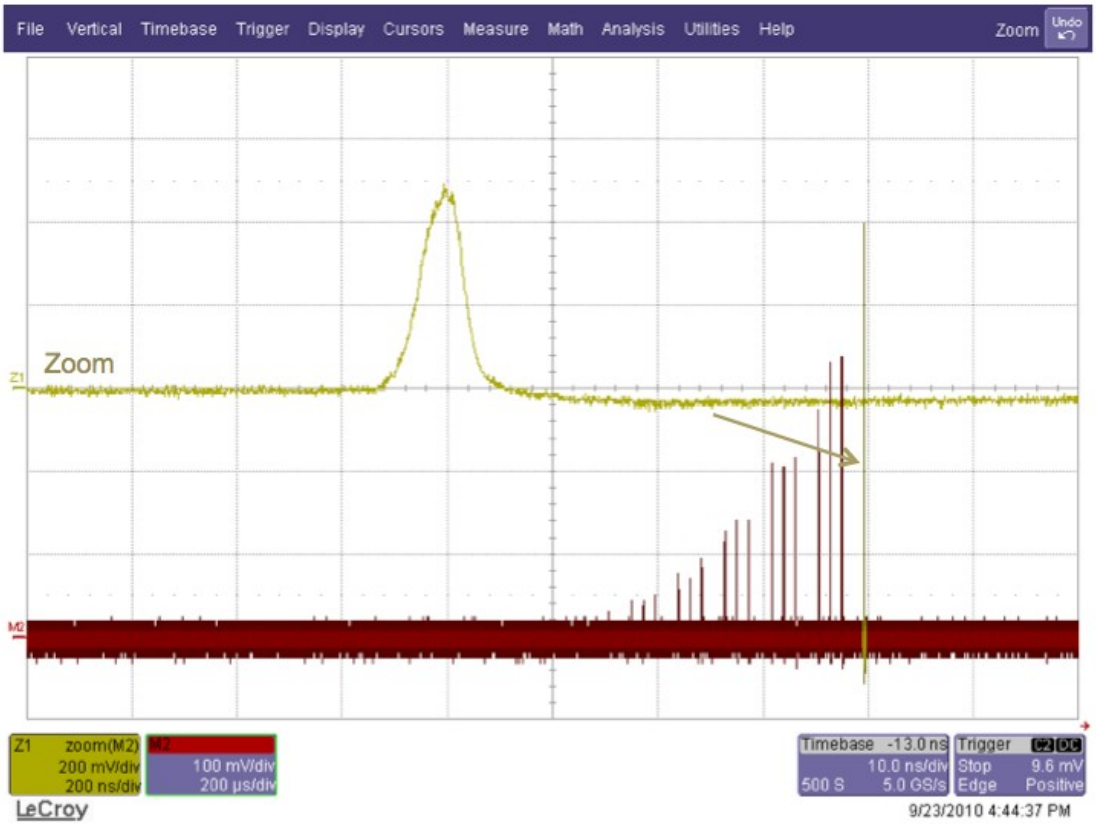

Figure 43: The loss pulse before the beam dump shows an amplitude of 0.5 V. Saturation of pre-amplifier, but not the diamond detector.

4.5 Example 5

Figures 44-47 analyse another unscheduled beam abort. Date: 16/10/2010 03:23:47

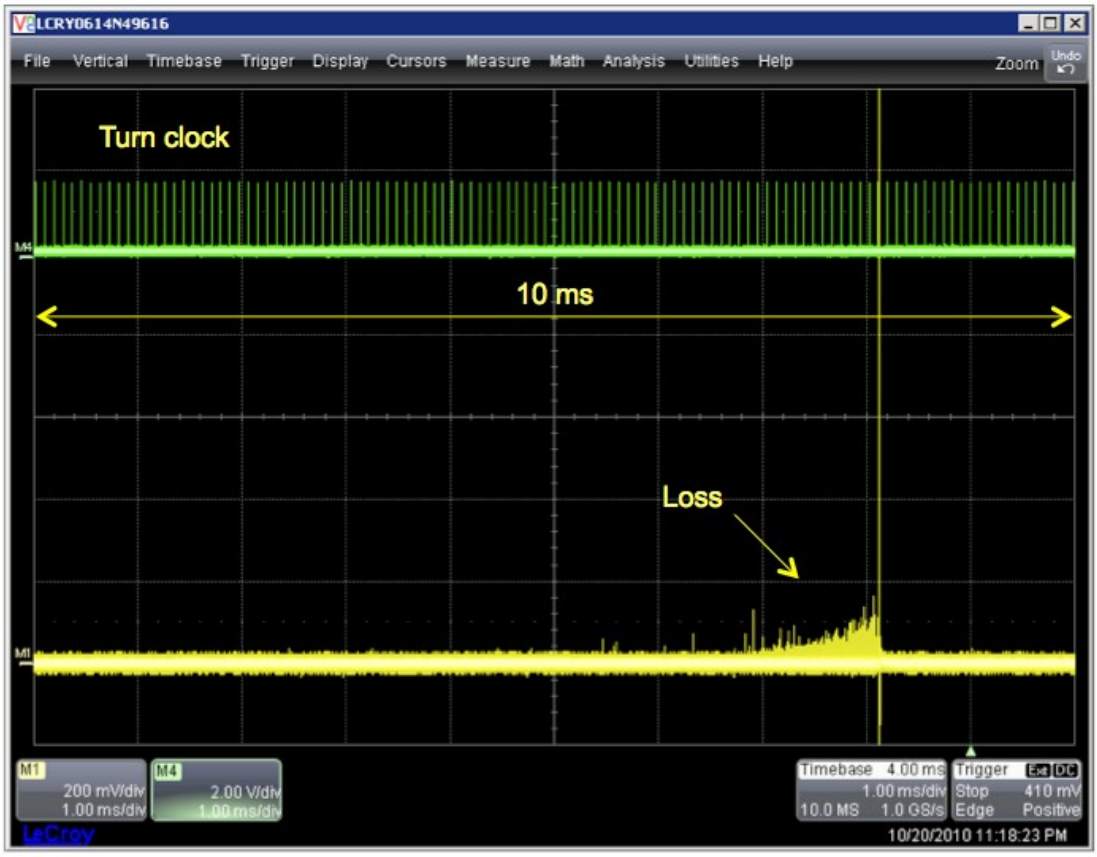

Figure 44: Beam loss structure shows a quadratic time profile.

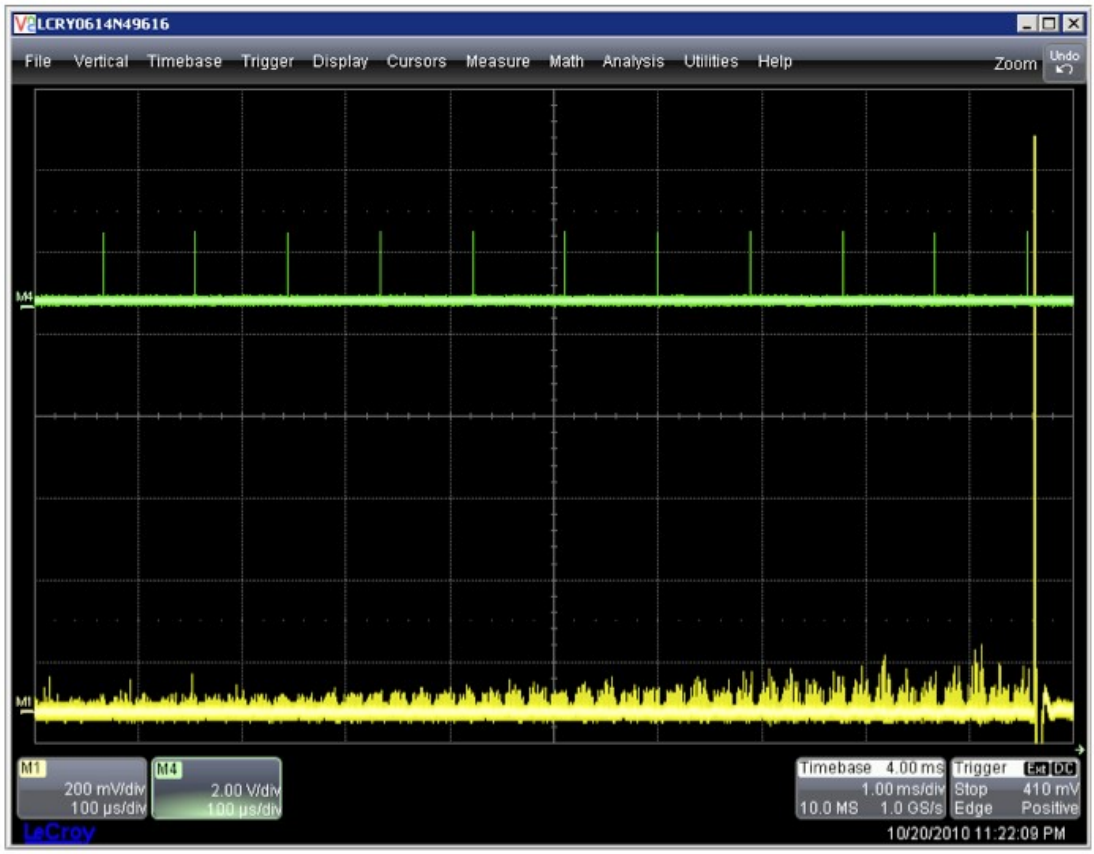

Figure 45: Time structure of the bunch trains and loss peak before beam dump.

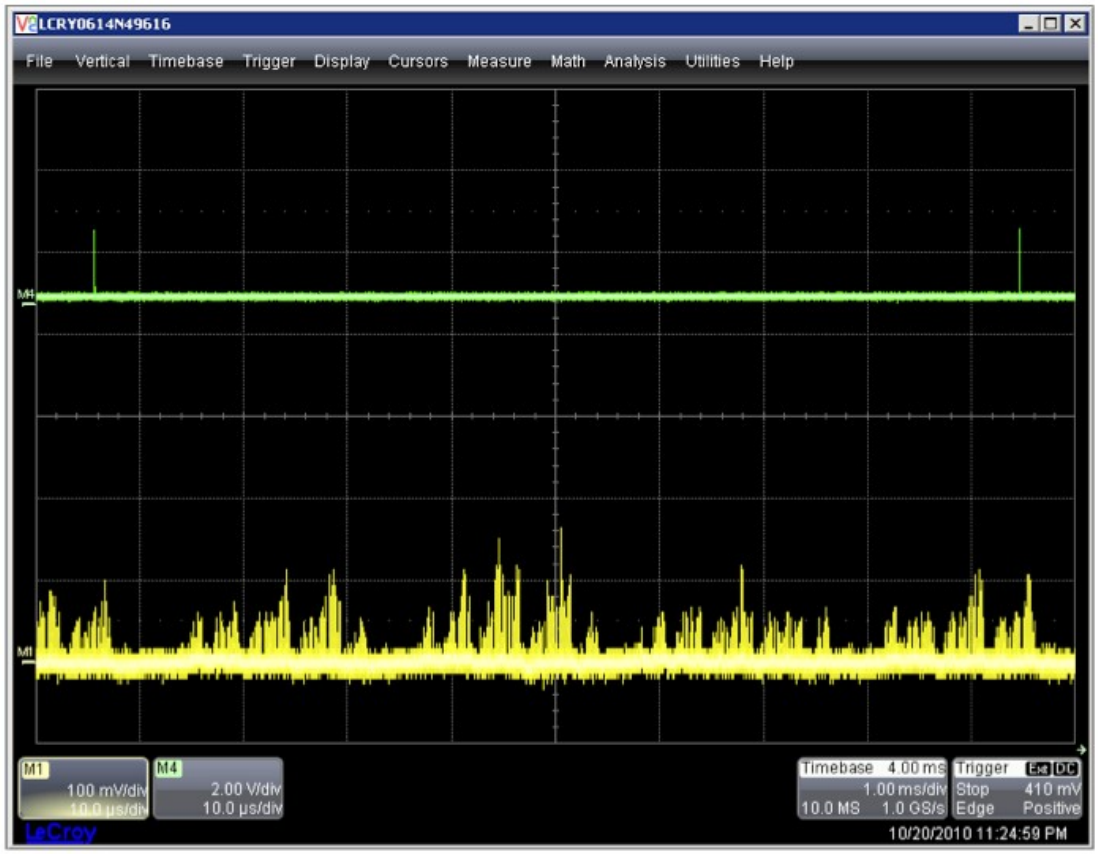

Figure 46: Bunch trains over one LHC period.

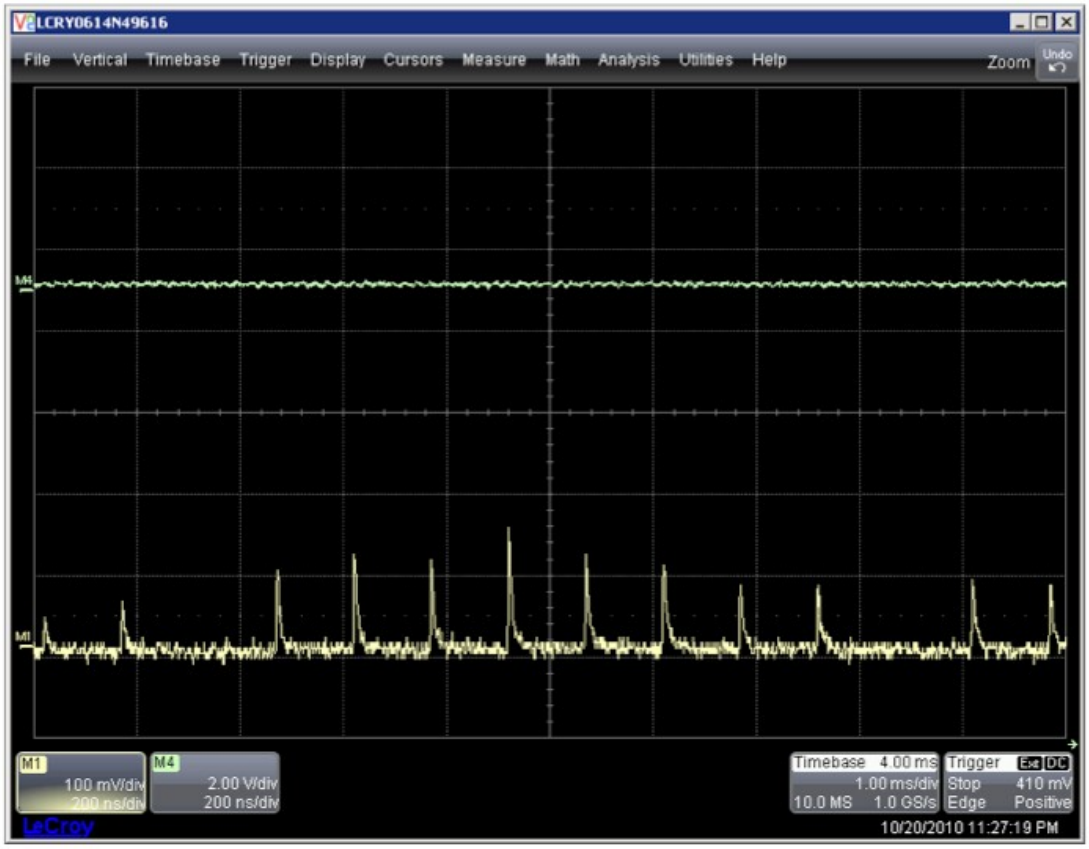

Figure 47: One bunch train contains 8 individual bunches which are separated by 150 ns.

* * *